Received: 22 October 2022 | Accepted: 21 July 2023

DOI: 10.1002/jev2.12355

RESEARCH ARTICLE

Neuron-derived extracellular vesicles contain synaptic proteins, promote spine formation, activate TrkB-mediated signalling and preserve neuronal complexity

Julia Solana-Balaguer[1,2] | **Genís Campoy-Campos**[1,2] | **Núria Martín-Flores**[1,2] | **Leticia Pérez-Sisqués**[1,2] | **Laia Sitjà-Roqueta**[1,2,3] | **Melike Kucukerden**[1,2,3] | **Ana Gámez-Valero**[1,4] | **Albert Coll-Manzano**[1,2,3] | **Eulàlia Martí**[1,4] | **Esther Pérez-Navarro**[1,2,3] | **Jordi Alberch**[1,2,3] | **Jordi Soriano**[5,6] | **Mercè Masana**[1,2,3] | **Cristina Malagelada**[1,2]

[1]Departament de Biomedicina, Institut de Neurociències (UBneuro), Universitat de Barcelona, Barcelona, Spain

[2]Centro de Investigación Biomédica en Red sobre Enfermedades Neurodegenerativas (CIBERNED), Madrid, Spain

[3]Institut d'Investigacions Biomèdiques August Pi i Sunyer (IDIBAPS), Barcelona, Spain

[4]Biomedical Research Networking Center for Epidemiology and Public Health (CIBERESP), Madrid, Spain

[5]Departament de Física de la Matèria Condensada, Universitat de Barcelona, Barcelona, Spain

[6]Universitat de Barcelona, Institute of Complex Systems (UBICS), Universitat de Barcelona, Barcelona, Spain

Correspondence
Julia Solana-Balaguer, Mercè Masana and Cristina Malagelada, Departament de Biomedicina, Institut de Neurociències, Facultat de Medicina i Ciències de la Salud, Casanova 143, north wing, 3rd floor, Universitat de Barcelona, Barcelona, 08036 Catalonia, Spain.
Email: juliasolana@ub.edu, mmasana@ub.edu and cristina.malagelada@ub.edu

Mercè Masana and Cristina Malagelada are co-senior authors.

Funding information
Spanish ministry of Universities; Ministerio de Ciencia e Innovación, Grant/Award Numbers: PID2020-119236RB-I00, PID2021-124896OA-I000, SAF2017-88812-R

Abstract

Extracellular vesicles (EVs) play an important role in intercellular communication as carriers of signalling molecules such as bioactive miRNAs, proteins and lipids. EVs are key players in the functioning of the central nervous system (CNS) by influencing synaptic events and modulating recipient neurons. However, the specific role of neuron-to-neuron communication via EVs is still not well understood. Here, we provide evidence that primary neurons uptake neuron-derived EVs in the soma, dendrites, and even in the dendritic spines, and carry synaptic proteins. Neuron-derived EVs increased spine density and promoted the phosphorylation of Akt and ribosomal protein S6 (RPS6), via TrkB-signalling, without impairing the neuronal network activity. Strikingly, EVs exerted a trophic effect on challenged nutrient-deprived neurons. Altogether, our results place EVs in the spotlight for synaptic plasticity modulation as well as a possible therapeutic tool to fight neurodegeneration.

KEYWORDS
extracellular vesicle, neuron, synapse, synaptic plasticity, TrkB

1 | INTRODUCTION

Extracellular vesicles (EVs) are small membrane-bound vesicles released by all cell types, which have been widely described to be involved in intercellular communication (Quek & Hill, 2017; Yáñez-Mó et al., 2015). Intercellular communication is an essential mechanism for higher processes in the CNS. Recently, EVs have been proven as versatile messengers in this context, since they are released from neurons, oligodendrocytes, astrocytes and other CNS cells (Budnik et al., 2016; Frühbeis et al., 2013, 2020; Holm et al., 2018; Rajendran et al., 2014; Schnatz et al., 2021), and contain proteins, RNAs, and lipids. Hence, EVs along with other transduction molecules, are necessary for healthy CNS maintenance, as they are biologically active when they reach the recipient cells (Gassama & Favereaux, 2021).

There are many types of EVs, distinguished by size, biogenesis, cellular origin and composition. Exosomes are 50–120 nm vesicles produced by the endosomal system and secreted by the fusion of multivesicular bodies with the plasma membrane. In contrast, microvesicles are bigger particles, between 100 nm and 1 μm released by outward budding from plasma membrane (Chuo et al., 2018; Takeuchi, 2021; Van Niel et al., 2018). As there are no available methods to fully separate exosomes from small microvesicles yet (Xu et al., 2016), we will refer to them by the general name of EVs (Gould & Raposo, 2013; Théry et al., 2018).

In neurons, EVs can be released by depolarization and calcium entrance and affect neuronal development and connectivity (Chivet et al., 2014; Sharma et al., 2019). Neuron-derived EVs have been characterized by the presence of neural cell adhesion molecule L1, as well as AMPA receptor subunits GluR2/3 (Fauré et al., 2006) and Arc mRNA and protein (Pastuzyn et al., 2018), which strongly suggest their potential role in the excitability of the recipient cells. Moreover, neuron-derived EVs enable the transfer of synaptotagmin 4, a pre-synaptic calcium sensor, which leads to pre-synaptic stimulation (Korkut et al., 2013).

In neurodegeneration, EVs can have a pathological role, as they can carry toxic molecules such as Amyloid-β (Rajendran et al., 2006), Tau (Wang et al., 2017) or α-synuclein (Emmanouilidou et al., 2010). However, little is known about neuron-derived EVs physiological functions in the CNS, and whether they can modulate synapses, signalling, and complex patterns of activity generated by neural circuitries. One of the signalling pathways involved in the maintenance of synapses in the CNS is BDNF-TrkB signalling (Horch & Katz, 2002). It has been recently described that BDNF-TrkB-containing endosomes induce synaptic changes in cortical neurons (Moya-Alvarado et al., 2023), but whether these endosomes come from internalized EVs remains unknown.

Moreover, specific neuron-derived EVs isolation from body fluids is not currently feasible, as its classic marker, L1CAM was recently found not to be associated with neuron-derived EVs (Norman et al., 2021).

For this reason, we focused this work on the study of the putative synaptic functions of neuron-derived EVs (Xia et al., 2022) isolated from cultured neurons. We found that cultured neurons internalized neuron-derived EVs at the soma and dendritic spines and that they contain synaptic proteins, which may be contributing to synapse formation or maintenance. Moreover, neuron-derived EVs activated Akt and RPS6 in recipient neurons via TrkB-mediated signalling and preserved neuronal complexity in the context of nutrient deprivation.

2 | MATERIALS AND METHODS

2.1 | Primary cortical cultures

Rat primary cortical cultures were prepared by dissecting out the cortex from embryonic day 18 (E18) Sprague-Dawley rats as previously described (Danzer et al., 2012; Martín-Flores et al., 2015). Cells were seeded on 0.25 mg/mL poly-L-lysine-coated (Sigma-Aldrich) plates (plated at a density of 900 cells/mm^2 or 750 cells/mm^2) or coverslips (300 cells/mm^2). Neurons were maintained in Neurobasal medium supplemented with B27 without serum (1:50), 2 mM GlutaMAX, and penicillin/streptomycin (all from Thermo Fisher Scientific). One-third of the medium was replaced every 7 days. Cell cultures were maintained in a 5% CO_2 atmosphere at 37°C. All experiments were performed at 13–14 DIV.

2.2 | Transfection

Bacteria containing the plasmid pCMS-eGFP (Addgene) were grown in Terrific Broth at 200 rpm and 37°C until saturation was reached. The commercial kit HiPure Plasmid Filter Midiprep Kit (Thermo Fisher Scientific) was used to isolate the plasmid. Transfection was carried out using Lipofectamine 2000 (Thermo Fisher Scientific) at DIV12, following the manufacturer's instructions.

2.3 | Isolation of EVs by sequential ultracentrifugation (UC), treatment and labelling

EVs were isolated from Neurobasal medium of cortical neurons at DIV13 (plated at a density of 900 cells/mm^2), as in Danzer et al. (2012), with minor modifications (Danzer et al., 2012). About 10 mL of medium was collected per plate and centrifuged at 300 × *g* for 5 min at room temperature (RT) to remove cell debris, and centrifuged again for 20 min at 2500 × *g* at 4°C to remove apoptotic bodies. Then, the supernatant (SN) was centrifuged for 30 min at 10,000 × *g* to discard large microvesicles (>500 nm). The SN was then ultracentrifuged for 2 h at 100,000 × *g* (4°C) and the subsequent pellet was washed with 1X PBS and ultracentrifuged again at 100,000 × *g* for 1 h. The resulting pellet contained the small EVs fraction, a fraction enriched in exosomes and small microvesicles.

Neurobasal medium supplemented with B27 without serum (1:50) and 2 mM GlutaMAX, in the absence of cells (EVs-free) was treated equally to obtain the negative control fraction (NegCT).

For protein content analysis the pellet was resuspended in loading buffer (Thermo Fisher Scientific) and loaded into western blotting (WB) gels.

For the EVs uptake analysis, EVs were labelled with MemGlow-560 (Cytoskeleton Inc.), as previously described (Boyer et al., 2020). MemGlow-560 is a fluorogenic probe which stably integrates into lipid membranes (Collot et al., 2019). EVs in 1X PBS were incubated with 200 nM MemGlow-560 for 1 h at RT. Two centrifuges at 10,000 × *g* for 15 min at 4°C were performed to pellet the excess of dye that was not linked to EVs membranes. The SN contained the labelled EVs and is used for treatment. Cultured neurons were treated with labelled EVs for 30 min. Labelled EVs were only used in Figure 2.

For EVs treatments, EVs were isolated in sterile conditions, and pellets were resuspended in sterile 1X PBS. Particle concentration was measured by Nanoparticle Tracking Analysis (NTA) (see Methods 2.5) and neuronal cultures were treated for 24 h with a ratio of 400 or 800 EVs:cell, which corresponds to ~0.8 μg or ~1.6 μg of protein, respectively, as measured by Micro BCA™ (Thermo Fisher Scientific). All experiments were performed at a ratio of 400 EVs:cell except the one in Figure S10.

2.4 | EVs isolation by size-exclusion chromatography (SEC)

As an alternative EVs isolation method, size exclusion chromatography (SEC) was applied, as described in Gámez-Valero et al. (2016), as follows. Neurobasal medium of cortical neurons at DIV13 was collected and centrifuged at 500 × *g* to discard cell debris, and at 2000 × *g* to discard apoptotic bodies. This SN was further concentrated by ultrafiltration (UF) using 100 KDa Amicon Ultra (Merck Millipore) at 2000 × *g*, obtaining a concentrated SN (cSN). EVs were then isolated by SEC. Briefly, the cSN was loaded on a Sepharose CL-2B (Sigma Aldrich) column, previously equilibrated with 1X PBS, and 35 fractions of 250 μL were collected. Protein concentration of each fraction was measured using the NanoDrop™ One microvolume UV–vis spectrophotometer (Thermo Fisher Scientific) and EVs-enriched fractions were identified using bead-based flow cytometry, as in Monguió-Tortajada et al. (2019) (see Methods 2.7). Fractions enriched in CD63 EV-marker were pulled together and considered as EVs-enriched. The following fractions, containing proteins, were also pooled and considered as EVs-free protein controls (ProtCT) (Figure S5A).

For EVs treatments, EVs were isolated in sterile conditions. Particle concentration was measured by NTA and neuronal cultures were treated for 24 h with a ratio of 400 EVs:cell, which corresponds to ~1.8 μg of protein, as measured by Micro BCA™ (Thermo Fisher Scientific).

2.5 | Nanoparticle tracking analyses (NTA)

EVs size and concentration were analysed by NTA, using NanoSight NS300 equipment (Spectris). Samples were diluted in 1X PBS and three videos of 60 s were recorded per sample. Videos were analysed with the NTA Software (NTA v3.4 Build 3.4.4) to determine the size and concentration of particles in EVs samples. Settings: Camera sCMOS, Laser Blue466, Camera Level 12, Slider Shutter 1200, Slider Gain 146, Shutter/ms 30, Frame rate/fps 25, Syringe Pump Speed/AU 50, Detection Threshold 5, Total Frames analysed 1498.

2.6 | Transmission electron microscopy (TEM)

EVs pellet was resuspended in 2% paraformaldehyde (PFA, Electron Microscopy Sciences) in 1X PBS and deposited on Formvar-carbon-coated 400-mesh copper grids for 25 min until adsorption. Grids were then transferred to a ~30 μL drop of 2% saturated aqueous uranyl acetate as a contrast agent. The excess mixture was removed by capillarity using filter paper and grids were washed in water. When dried, samples were observed under a JEOL JEM-1010 (100 kV) microscope (JEOL, Ltd.) and image acquisition was made with a Gatan Orius CCD Camera (AMETEK, Inc.) at 200,000× magnification.

2.7 | Bead-based flow cytometry

SEC fractions were assessed by flow cytometry to identify the EVs-marker CD63, as previously reported (Gámez-Valero et al., 2016; Monguió-Tortajada et al., 2019). Briefly, each fraction was incubated with aldehyde/sulphate-latex beads (Invitrogen) for 15 min at RT. Bead-coupling buffer (1X PBS with 0.1% BSA and 0.01% NaN3, all from Sigma-Aldrich) was added to each fraction, and fractions were left on rotation O/N. A centrifuge of 2000 × *g* for 10 min was used to pellet the EVs-coated beads. An additional centrifugation was performed after adding BCB in order to wash the samples. EVs-coated beads were labelled with anti-CD63 antibody (1:100, BD Biosciences, #551458) for 30 min at 4°C. After washing with BCB, samples were incubated with FITC-conjugated secondary goat anti-mouse antibody (1:100, Southern Biotech, #1032-02) for 30 min at 4°C. Then, samples were washed with BCB, with a centrifuge of 2000 × *g* for 10 min, and each fraction was resuspended with 120 μL of 1 X PBS. Samples were then analysed by flow cytometry in a BD LSRFortessa (BD Biosciences) using the BD FACSDiva™ Software. A total of 10,000 beads (events) were acquired for each sample and the median fluorescence intensity (MFI) was obtained.

2.8 | Western blotting (WB)

Whole-cell extracts were lysed and centrifuged at 14,000 × *g* to remove cell debris. Protein concentration was measured using Bradford reagent (Bio-Rad), following the manufacturer's instructions. The protein concentration of EVs samples derived from the medium of three P100 plates was measured using Micro BCA™ (Thermo Fisher Scientific), following the manufacturer's instructions.

Samples were loaded in 4%–12% polyacrylamide gels (NuPAGE™ Novex™ 4%–12% Bis-Tris) with a molecular marker (PageRuler™ Prestained Protein Ladder) and were run with NuPAGE™ MOPS SDS Running buffer. The transference to a nitrocellulose membrane was performed using iBlot2® Transfer Stack supports (all from Thermo Fisher Scientific).

The following primary antibodies were used (1:1000 it not stated otherwise): mouse monoclonal anti-Alix (1:500, Cell Signalling Technology, #2171), mouse monoclonal anti-TrkB (BD Biosciences, #610102), rabbit polyclonal anti-calnexin (Abcam, #ab22595), mouse monoclonal anti-PSD95 (Thermo Fisher Scientific, #MA1-045), rabbit polyclonal anti-p75 (Promega, #G323A), rabbit polyclonal anti-VGLUT-1 (Synaptic Systems, #135303), mouse monoclonal anti-Flotillin-1 (BD Biosciences, #610821), mouse monoclonal anti-TSG101 (Abcam, #ab83), mouse polyclonal anti-BDNF (Icosagen, #327-100), rabbit monoclonal anti-phospho RPS6 (Ser235/236) (Cell Signalling Technology, #4858), mouse monoclonal anti-RPS6 (Cell Signalling Technology, #2317), rabbit monoclonal anti-phospho Akt (Ser473) (Cell Signalling Technology, #4060), rabbit monoclonal anti-Akt (Cell Signalling Technology, #4691), rabbit monoclonal anti-phospho TrkB (Tyr706) (1:500, Signalway Antibody #11328), rabbit monoclonal anti-phospho GluA1 (Ser831) (Merck, #08-823), rabbit polyclonal anti-GluA1 (Merck, #ABN241), mouse monoclonal anti-phospho-ERK1/2 (Thr202/Tyr204) (Cell Signalling Technology, #9106), rabbit polyclonal anti-ERK (Santa Cruz Biotechnology, #sc-93), rabbit polyclonal anti-phospho-PKC α/β II (Thr638/641) (Cell Signalling Technology, 9375), rabbit polyclonal anti-PKCα (Cell Signalling Technology, #2056), rabbit polyclonal anti-phospho-p70 S6 kinase (Ser371) (Cell Signalling Technology, #9208), rabbit polyclonal anti-p70 S6 kinase (Cell Signalling Technology, #9202), rabbit monoclonal anti-phospho-4E-BP1 (Thr37/46) (Cell Signalling Technology, #2855) and rabbit monoclonal anti-4E-BP1 (Cell Signalling Technology, #9644). Membranes were incubated with the antibodies for 16 h at 4°C in agitation.

Anti-actin antibody conjugated to horseradish peroxidase (1:100,000, Merck, #A3854) was incubated for 30 min at RT and used as loading control.

Anti-mouse and anti-rabbit secondary antibodies produced in goat and conjugated to horseradish peroxidase (1:10,000, Thermo Fisher Scientific, #31430 and #31460, respectively) were incubated for 1 h at RT.

Chemiluminescent images were acquired using a Chemidoc imager (BioRad) and quantified by computer-assisted densitometric analysis (ImageJ). To remove the signals and allow the incubation with other antibodies the Restore™ PLUS Western Blot Stripping Buffer (Thermo Fisher Scientific) was used.

2.9 | Calcium fluorescence imaging

2.9.1 | Calcium imaging recordings

Spontaneous neuronal activity was measured at DIV14 through calcium imaging, as previously described (Fernández-García et al., 2020; Montalà-Flaquer et al., 2022). Briefly, neuronal cultures were seeded in 12 mm coverslips in P24 plates at a density of 160,000 cells/cm^2. At DIV14, 1 μL of 1 mM Fluo4-AM calcium indicator (dissolved in DMSO) was added to the culture and incubated for 20 min at 37°C (final concentration 1 μM). After incubation, cultures were transferred to an observation chamber (P35G-0-14-C; MatTek Corporation) filled with external medium containing: HEPES (10 mM), NaCl, (128 mM), KCl (4 mM),

glucose (10 mM), sucrose (45 mM), $CaCl_2$ (2 mM) and $MgCl_2$ (1 mM), pH 7.4. Recordings were performed on an Olympus IX70 inverted microscope in combination with a Hamamatsu Orca Flash 4.0 V2 camera (Digital CMOS camera C11440-22CU) with a Dual OptoLED power supply (Cairn Research Ltd.). Images were obtained at a rate of 20 frames per second (fps), with a 5× magnification objective at RT for 10 min. At the end of the recording, highly-quality images were obtained at 2 fps for 1 min to facilitate the identification of Regions of Interest (ROIs) in subsequent analysis.

2.9.2 | Calcium imaging analysis

Analysis of calcium images was performed as described (Fernández-García et al., 2020) using the NETCAL software (www.itsnetcal.com) (Orlandi et al., 2017). Briefly, ROIs representing individual cells were automatically detected from the highly-quality images, and the fluorescent traces from each ROI in the culture were automatically extracted. Spikes were reconstructed from raw calcium traces using the MLspike algorithm, with a decay time (Tau) of 1 s and an amplitude (A) of 0.1. These data were visualized in the form of raster plots and were used to obtain the number of ROI, mean number of spikes, mean inter-spike interval (ISI), and mean inter-burst-interval (IBI) from each culture. Additional custom-made MATLAB code was used to analyse coordinated neuronal activity. For that, raster plots were scanned with a moving window 2 s wide and 0.1 s step, summing up all neuronal activations present in the window without repetition. The resulting signal varied between 0 (no activity) and 1 (all neurons in the network activating in unison). Sharp peaks in this signal revealed strong coordinated activity that was associated with network bursts. Significant bursting events were those peaks whose amplitude was above 0.05 (5% of the network active). The percentage of active neurons, network IBI and population activity (PA) was computed from the network burst data.

2.10 | Cell culture treatments

To block EVs-uptake, 5 μM chlorpromazine (CPZ, Sigma-Aldrich, #C8138) (in MilliQ water) and 80 μM dynasore (Dyn, Sigma-Aldrich, #324410) (in DMSO) were used. Neurons were treated with the inhibitors for 30 min prior to the addition of EVs.

To inhibit TrkB specifically in EVs, Neurobasal medium of cultured cortical neurons at DIV13 was collected and 100 μM ANA-12 (Merck, #SML0209, in DMSO) was added. After 1 h, EVs were isolated following the UC protocol (see Methods 2.3).

For nutrient-deprivation analysis, Neurobasal medium lacking the B27 supplement was applied to neurons for 24 h (NB-B27). As a control, sister cultured neurons were maintained in Neurobasal complete medium (NBC).

2.11 | Immunocytochemistry and image analyses

Rat primary cortical neurons were fixed with 4% paraformaldehyde in 1X PBS and stained as previously described (Martín-Flores et al., 2015). Briefly, samples were permeabilized with Superblock-PBS (Thermo Fisher Scientific) with 0.25% Triton X-100 (Sigma-Aldrich) and blocked with Superblock-PBS. The following primary antibodies were used: chicken polyclonal anti-GFP (1:500, Synaptic Systems, #132006), mouse monoclonal anti-PSD95 (1:50, Thermo Fisher Scientific, #MA1-045), rabbit polyclonal anti-VGLUT-1 (1:100, Synaptic Systems, #135303), mouse monoclonal anti-MAP-2 (1:500, Abcam, #ab11268) and rabbit polyclonal anti-GFAP (1:500, Proteintech, #16825-1-AP).

The following secondary antibodies (all obtained from Thermo Fisher Scientific) were used: goat anti-chicken Alexa Fluor 488 (1:500, #A11039), goat anti-mouse Alexa Fluor 568 (1:500, #A11019), goat anti-rabbit Alexa Fluor 633 (1:500, #A21072), goat anti-rabbit Alexa Fluor 488 (1:500, #A11070), goat anti-mouse Alexa Fluor 488 (1:500, #A11017) and Phalloidin Alexa Fluor 647 (1:500, #A22287). Hoechst 33342 (1:5,000, Thermo Fisher Scientific, #H3570) was used to stain nuclei. Coverslips were mounted with ProLong® Gold Antifade Mountant (Thermo Fisher Scientific).

For EVs uptake analysis, images were acquired with a ZEISS LSM880 confocal microscope as z-stacks (five slices in a range of 5 μm) with a 63× magnification. Images in the z-stack were processed with ImageJ as Z-projects. Colocalization analysis was carried out with Image calculator module, in which the colocalizing dots (EVs) inside the neurons are shown. With the GFP channel, two masks were created, one for the neuronal soma (Soma Mask) and the other for all neuron (Cell Mask). The subtraction of the soma resulted in a mask for the neurites (Neurite Mask). The percentage of colocalizing dots (EVs) were analysed in both areas. The colocalizing ratio was calculated as [Area of colocalizing dots in the soma or dendrites]/[Area of EVs in the Neuron]. Orthogonal views (YZ and XZ) were also used to show the colocalizing EVs inside the neuron. At least five neurons of three independent neuronal cultures were analysed.

For dendritic spine analysis, cells were visualized with the ZEISS LSM880 confocal microscope, using the 63× objective with a 2× digital zoom and single-plane images were analysed. For each condition, at least eight neurons from three independent cultures were quantified. For spine density, five primary dendrites were analysed per neuron, and spines were counted manually using Image J. PSD-95 and VGLUT-1 puncta in dendrites were quantified using Cell Profiler cell image analysis software

(www.cellprofiler.org, Broad Institute) (Carpenter et al., 2006; Stirling et al., 2021). Briefly, dendrites were identified and were used to mask PSD-95 and VGLUT-1 channels, to select only puncta present in dendrites. Measures of mean intensity and shape of PSD-95 and VGLUT-1 puncta were obtained. To identify clusters of PSD-95 and VGLUT-1, the *RelateObjects* module was used, and the number of clusters was normalized by the area of the dendrites taken per neuron.

To improve images visualization, images were adjusted with Photoshop® to potentiate the brightness and reduce the background and the same settings were used in all the conditions.

For the branching analysis, images of different fields of the neuronal culture containing many neurons, were acquired with a ZEISS Axio Observer Z1 fluorescence microscopy with a 20x magnification. Using Cell Profiler software, neurites of all neurons present in the image were subtracted to get the neuronal soma, and somas were identified as independent objects. Neurites were then enhanced using the enhancement method 'line structures' and turned into a binary image. From this image, and using the neuronal soma as input, neurons were identified as independent objects. Objects touching the border of the image were discarded. Neuron objects were used to mask the binary image of enhanced neurites. From this masked image, the morphological skeleton was generated with *Morph* module. Measurements of endpoints (termini branches), trunks (primary dendrites), and total tree length were obtained per neuron, using the *MeasureObjectSkeleton* module. Neurons from 5 fields per coverslip were analysed and the mean of all neurons per field was acquired.

For neuron viability analysis, nuclei were identified as independent objects. A mask with neuronal soma was used to obtain only neuronal nuclei. Nuclei classification into viable or apoptotic was based on intensity, intensity distribution, size and shape, texture and granularity parameters, using machine learning in Cell Profiler Analyst software (Jones et al., 2008, 2009; Stirling et al., 2021).

In all cases, the same Cell Profiler pipeline was used to process all the images, following identically the same steps.

For the quantification of the purity of neuronal cultures, 100 images covering almost all cell-plated coverslip were acquired with a Widefield AF600 Monochroma Camera Leica fluorescence microscope with a 20× magnification, and images were processed as a mosaic. MAP-2 and GFAP positive cells were selected and counted using *AnalyseParticles* module of ImageJ.

2.12 | Statistical analysis

All experiments were performed at least using three independent neuronal cultures, unless otherwise stated in the figure legend, and data of each culture replicate was asserted as mean ± SEM. Normal distribution was considered when all the data passed one of the following normality tests: D'Agostino-Pearson, Shapiro-Wilk, and Kolmogorov-Smirnov. When two conditions were compared, analyses were performed using the unpaired two-sided Student's *t*-test (95% confidence) (Figures 2,5, S1 and S4). When Gaussian distribution was not assumed (Figure 3A and B), statistics were performed using the Mann-Whitney *U* test. When three conditions were compared, one-way ANOVA with Bonferroni's post hoc test was performed (Figures 4 and S5). When four conditions were compared, two-way ANOVA with Bonferroni's post hoc test was performed (Figures 5, S9 and S10). *F*-test was used to examine variances prior to pairwise comparisons. To detect significant outlier values, Grubbs' and ROUT tests were used. Values of $P < 0.05$ were considered statistically significant. Data were processed and analysed blindly.

3 | RESULTS

3.1 | Isolation and characterization of EVs derived from cultured cortical neurons

To investigate the putative role of neuron-derived EVs, we first validated our isolation protocol by checking vesicles' population and protein content. We purified EVs from Neurobasal medium from mature cultured cortical neurons by sequential UC, by which we discarded cell debris, apoptotic bodies (P2000) and large EVs (P10K) and obtained the small EVs (sEVs) (Figure 1A). NTA revealed the expected size of small EVs (exosomes and small microvesicles) with sizes ranging from approximately 50–500 nm, and with a size average of 115 nm (Figure 1B). TEM images of negatively stained EVs confirmed this finding, showing a heterogenous population of EVs containing different sizes and the described cup-shaped structure of EVs (Jung & Mun, 2018) (Figure 1C). Our cortical cultures consisted in a 90% of neurons and only a 10% of astrocytes (Figure S1), consistent with other works (Lindholm et al., 1993; Pfrieger & Barres, 1997). These suggest that the effect of astrocytic EVs is minimal compared to neuronal EVs.

By WB analysis, we confirmed that our EVs fraction was enriched in the EVs markers TSG-101, Flotillin-1, and Alix, and small levels of the negative marker calnexin-1, in comparison with the initial total lysate. Unexpectedly, we found that the EVs fraction contained the neuron-specific presynaptic protein VGLUT-1 and the postsynaptic protein PSD-95. Enriched levels of TrkB, p75 and BDNF, which have been extensively linked with synaptic processes (Chapleau & Pozzo-Miller, 2012; Zagrebelsky et al., 2020; Zanin et al., 2019), were also detected in the EVs fraction (Figure 1D), suggesting a plausible synaptic effect of EVs on neighbouring neurons.

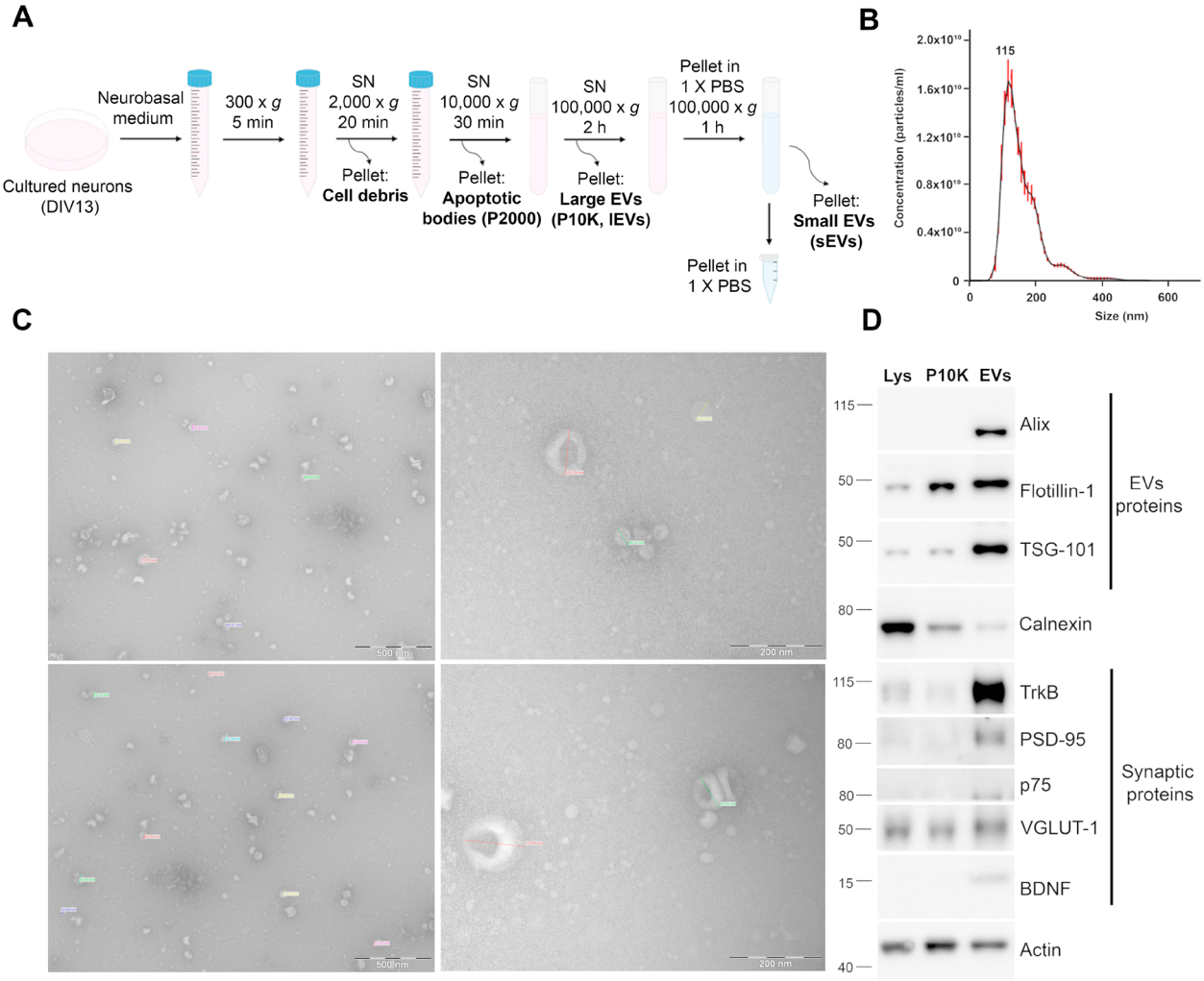

FIGURE 1 EVs derived from cortical neurons are enriched in synaptic proteins. EVs were isolated from cortical neurons culture media at DIV13 following a sequential UC protocol. (A) Schematic representation of the EVs isolation procedure. Cell debris, apoptotic bodies (P2000) and large EVs (P10K) were discarded during the isolation process, and small EVs (sEVs) were obtained. SN, supernatant. (B) Size distribution of particles by NTA. Red lines indicate the standard deviation. 115 nm represents the most frequent particle size. (C) TEM micrographs show particles with the characteristic morphology and size of small EVs. (D) Samples were subjected to WB and EVs markers (Alix, Flotillin-1, TSG-101) and synaptic proteins (TrkB, PSD-95, p75NTR, VGLUT-1 and BDNF) were analysed. Calnexin was used as an EVs negative control. Lys, neuronal lysate. Full length WB can be found in Figure S12.

To validate this finding, we isolated EVs with an alternative method, following UF and SEC (Figure S2A). The SEC elution profile revealed a peak enriched in vesicles positive for CD63 (from fractions F11–F13) (Figure S2B). EVs size and shape were confirmed by NTA measure (Figure S2C) and TEM (Figure S2D). The CD63 negative fractions that eluted after this EVs-enriched peak, contained a high protein concentration and were also pooled and used a protein control (protCT, from fractions F15–F17) (see Figure S5). By WB, we confirmed that SEC-isolated EVs were enriched in markers such as Alix, Flotillin-1 and TSG101. Importantly, using this second method of EVs isolation, we also found that EVs contained the synaptic proteins TrkB, PSD-95, p75, VGLUT-1 and BDNF (Figure S2E).

With a fluorogenic membrane probe (Memglow™-560) we labelled EVs (in red), and confirmed their internalization by neurons (in green, eGFP+), 30 min after treatment (Figure 2A). Indeed, MemGlow-560™ specifically bound to EVs' membranes as no fluorescent signal was detected within neurons when cultures were treated with 1X PBS with MemGlow-560™ (Figure 2B). The neuronal somas internalized most of the EVs (78.5%) compared to dendrites (21.5%) probably due to the differential area. Interestingly, 62% of the eGFP+ neurons showed EVs internalization at the dendritic spines suggesting a specific local effect (Figures 2A and S3).

EVs are typically internalized into the endosomal compartment by endocytosis. However, the exact endocytic mechanism used to internalize neuron-derived EVs has not been assessed yet. To investigate whether EVs endocytosis was dynamin dependent, including clathrin-dependent endocytosis (CME), we treated cultures with an inhibitor of the CME (chlorpromazine, CPZ) (Francia et al., 2019) or with a dynamin inhibitor (dynasore, Dyn) (Preta et al., 2015), 30 min prior to the addition of

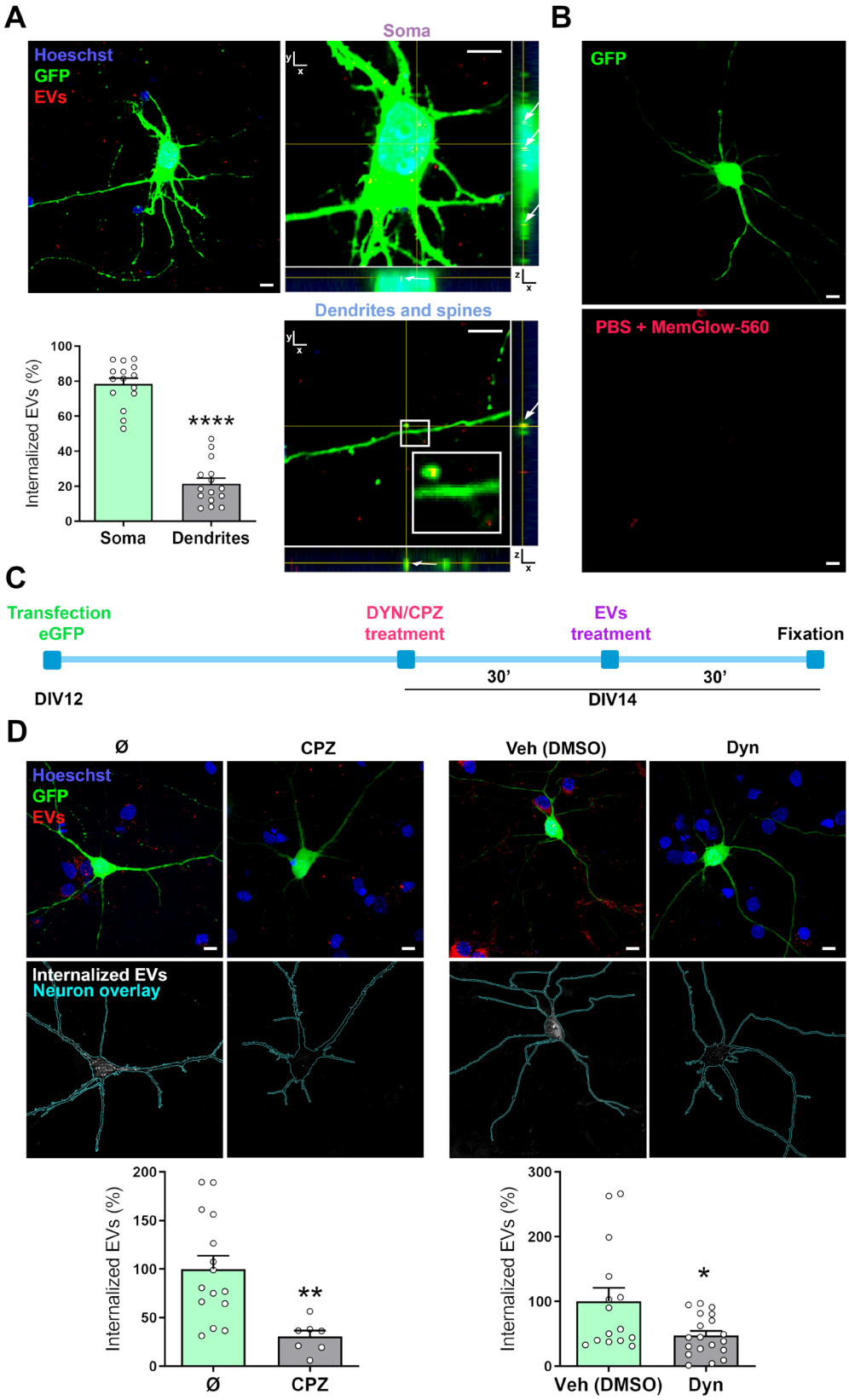

FIGURE 2 Neuron-derived EVs are taken up both in the soma and dendrites and their internalization is mediated by clathrin-dependent endocytosis. Cultured neurons were transfected at DIV12 with an eGFP plasmid (in green). EVs were isolated from sister neuronal cultures and labeled with MemGlow-560 (in red). (A) Orthogonal views show EVs-uptake in the soma, in dendrites, and also in dendritic spines. The graph shows the percentage of internalized EVs in the soma and in the dendrites. (B) Memglow-560 specifically labels EVs, as when used to label non-EVs samples (only 1X PBS) there was no fluorescent signal. (C) Experimental design to assess the internalization mechanism of EVs in recipient neurons. EVs used for treatment were isolated from sister cultured neurons at DIV13. eGFP-transfected neurons were treated with uptake-inhibitors CPZ (5 μM) and Dyn (80 μM) 30 min prior to EVs treatment. (D) Representative

(Continues)

FIGURE 2 (Continued)

images showing EVs-uptake in neurons. Images in the z-stack are processed with Image-J as Z-Projects. Images below show the colocalization dots between both channels, which represent EVs that have been internalized by neurons. The graphs show the percentage of internalized EVs per neuron. Ø = No treatment; CPZ = Chlorpromazine; Vehicle = DMSO; Dyn = Dynasore. Scale bar of 5 μm in all the images. Values represent different neurons (≥ 5 per experiment) from three independent neuronal cultures (mean ± SEM). Data was analysed by Student's *t*-test (****$P < 0.0001$ vs. soma, *$P < 0.05$ vs. Veh, **$P < 0.01$ vs. Ø).

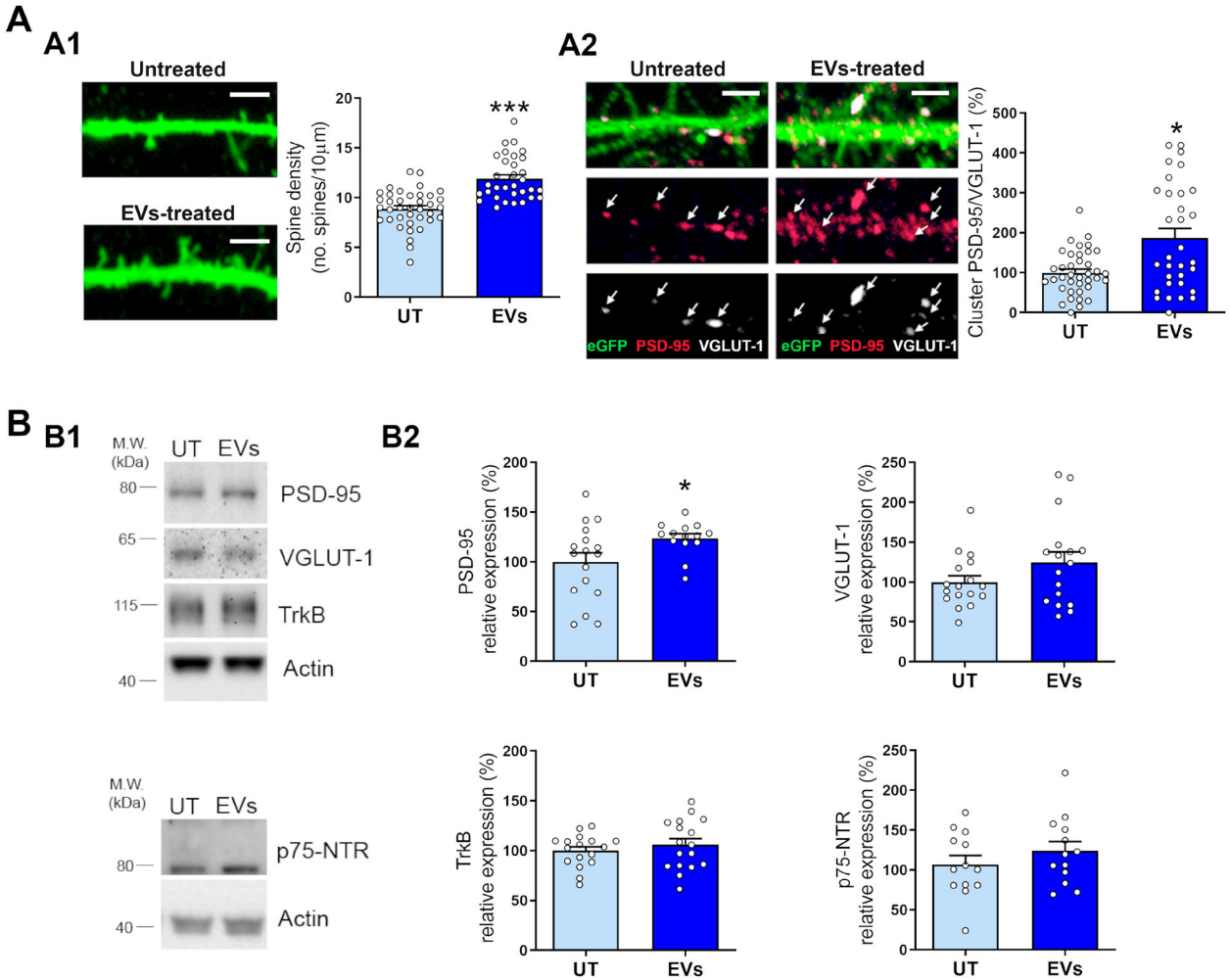

FIGURE 3 EVs derived from cortical neurons exert a direct modulation of synapses. Cultured cortical neurons were treated with EVs for 24 h. (A) (A1) Representative images of dendritic spines in neurons untreated (UT) or treated with EVs (EVs). Scale bar of 2 μm. The graph shows the spine density quantification (n° of spines/10 μm). Spines were counted in 10 μm and five dendrites per neuron were quantified. The mean of all dendrites per neuron is represented. (A2) Representative images of VGLUT-1 and PSD-95 clusters. The graph shows the quantification of clusters of PSD-95 and VGLUT-1 co-localization in dendrites. Values represent different neurons (≥8 per experiment) from three independent neuronal cultures. (B) (B1) Neurons UT or EVs-treated were lysed and subjected to WB analysis. (B2) Densitometric analysis of synaptic proteins PSD-95, VGLUT-1, TrkB and p75NTR. Actin was used as a loading control. Values represent culture replicates of three independent neuronal cultures (mean ± SEM). Full length WB can be found in Figure S12. Data was analysed by Student's *t*-test in A1 and by Mann-Whitney test in A2 and B (*$P < 0.05$, ***$P < 0.001$ vs. UT).

EVs (Figure 2C). EVs uptake was considerably reduced after treatment with CPZ (to a 30.5%) or Dyn (to a 47.5%), confirming that EVs internalization depends on CME (Figure 2D).

3.2 | Neuron-derived EVs induce spine formation in recipient neurons and activate BDNF-TrkB-mediated signalling

To assess whether neuron-derived EVs could modulate excitatory synaptic function, cultured cortical neurons were treated with them for 24 h. We observed by immunofluorescence (IF) that EV-treated neurons exhibited an increased number of spines (Figure 3A1) and an elevation of excitatory synapses, assessed as the increased number of PSD-95/VGLUT-1 clusters (Figure 3A2).

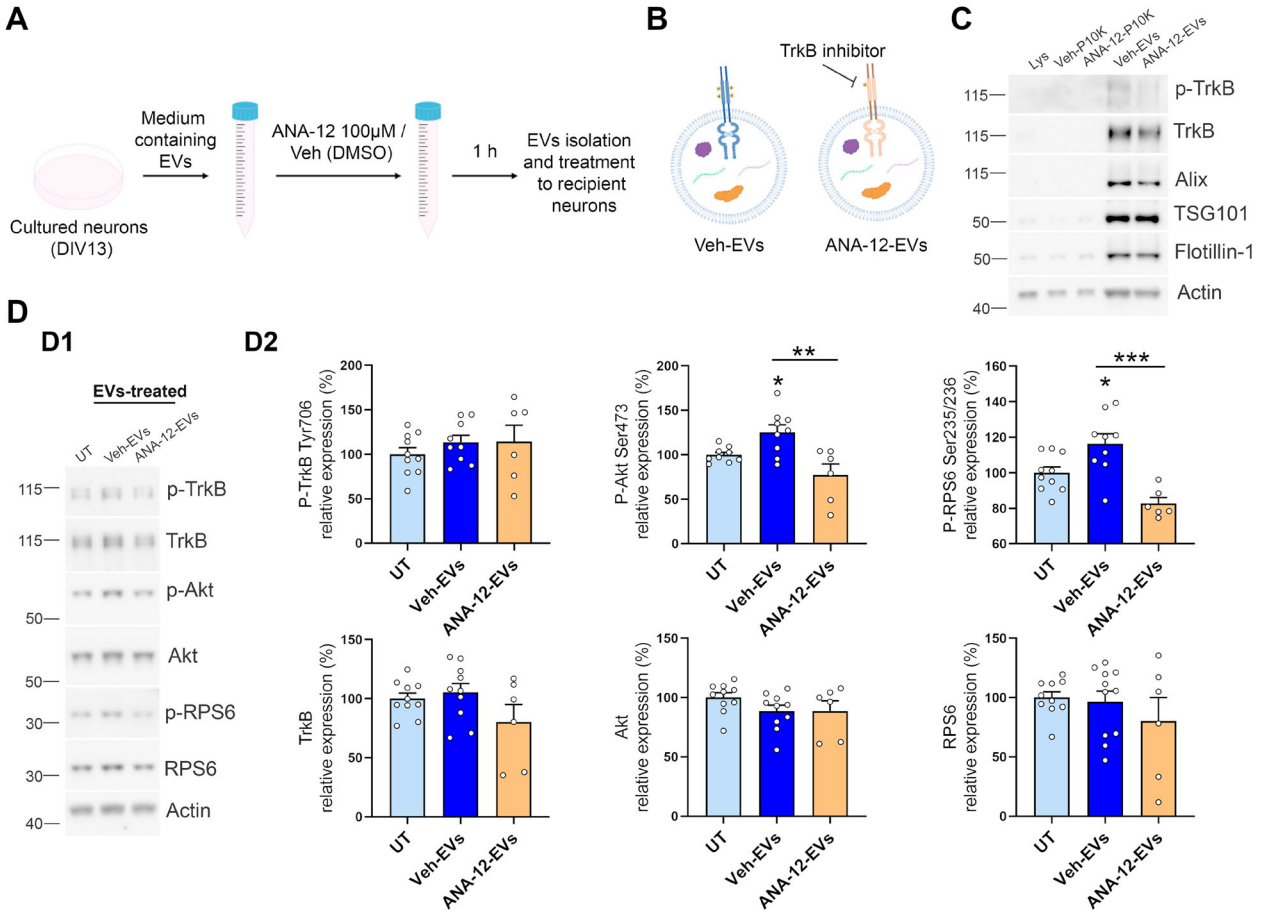

FIGURE 4 Neuron-derived EVs activate Akt and RPS6 via TrkB-mediated signalling. (A) Schematic overview of the experimental procedure. Neurobasal medium from DIV13 cortical neurons was collected and the EVs-containing medium was treated with 100 μM ANA-12 or DMSO as vehicle (Veh) for 1 h. EVs were isolated following sequential UC. (B) Representation of Veh-EVs, with active TrkB as a cargo, and ANA-12-EVs, with diminished TrkB phosphorylation. (C) Neuronal lysates, P10K and EVs samples (Veh or ANA-12) were subjected to WB and EVs markers (Alix, Flotillin-1, TSG-101), phosho-Tyr706-TrkB and total TrkB were analysed. (D) Cultured cortical neurons were treated with Veh-EVs or ANA-12-EVs for 24 h. (D1) Neurons UT or EVs-treated were lysed and subjected to WB analysis. (D2) Densitometric analysis of phospho-Tyr706-TrkB, phospho-Ser473-Akt, phospho-Ser235/236-RPS6, and total levels of TrkB, Akt and RPS6. Actin was used as a loading control. Values represent culture replicates of three independent neuronal cultures (mean ± SEM). Full length WB can be found in Figure S12. Data was analysed by One-way ANOVA (**$P < 0.01$ vs. Veh-EVs and ***$P < 0.001$ vs. Veh-EVs).

Besides, PSD-95 or VGLUT-1 puncta were increased after EVs treatment (Figure S4A,B). Nonetheless, PSD-95 or VGLUT-1 levels (mean intensity), as a readout of synaptic strength of the individual spines, and the area of the clusters, as a readout of spine maturation (Arellano et al., 2007; Béïque & Andrade, 2003; Pérez-Sisqués et al., 2021), remained unaltered (Figure S4C–E). This might indicate that, although EVs-treatment increases the number of synapses, it might not trigger their consolidation.

This result was validated with EVs isolated by SEC (Figure S5). Similar to our previous findings (Figures 3A 2 and S4), EVs increased the number of PSD-95/VGLUT-1 clusters in recipient neurons, without altering their area. PSD-95 puncta were also increased after the treatment, with no effect on VGLUT-1.

Importantly, the protein enriched fraction (ProtCT) and the EVs-negative control (NegCT, obtained from cell media not incubated with cells), did not exert any synaptic effect, as expected (Figures S5B-C and S6A-B).

Back to UC-isolated EVs, we confirmed by WB our IF analyses (Figure 3), and after EVs-treatment, recipient neurons showed higher levels of PSD-95, with no changes in VGLUT-1. Levels of TrkB and p75-NTR proteins remained unaltered after the treatment (Figure 3B).

Given that we found that neuron-derived EVs were enriched in TrkB and BDNF (Figures 1D and S2E), we investigated whether TrkB present in EVs mediated the activation of the BDNF-TrkB receptor signalling in recipient neurons. For this, culture media containing EVs was incubated with 100 μM of the TrkB-inhibitor ANA-12 (Cazorla et al., 2011) and EVs were isolated after 1 h (Figure 4A). We first confirmed that ANA-12 inhibited TrkB activity by detecting decreased levels of phospho-TrkB in EVs (Figure 4B,C). Next, we observed that control EVs (treated with DMSO as vehicle (Veh-EVs)) could effectively increase the levels of phospho-Akt and phospho-RPS6, downstream effectors of TrkB signalling (Fahnestock & Nicolini, 2015), in recipient neurons. However, EVs treated with ANA-12 (ANA-12-EVs), were unable to induce this effect (Figure 4D). Veh-EVs effect was

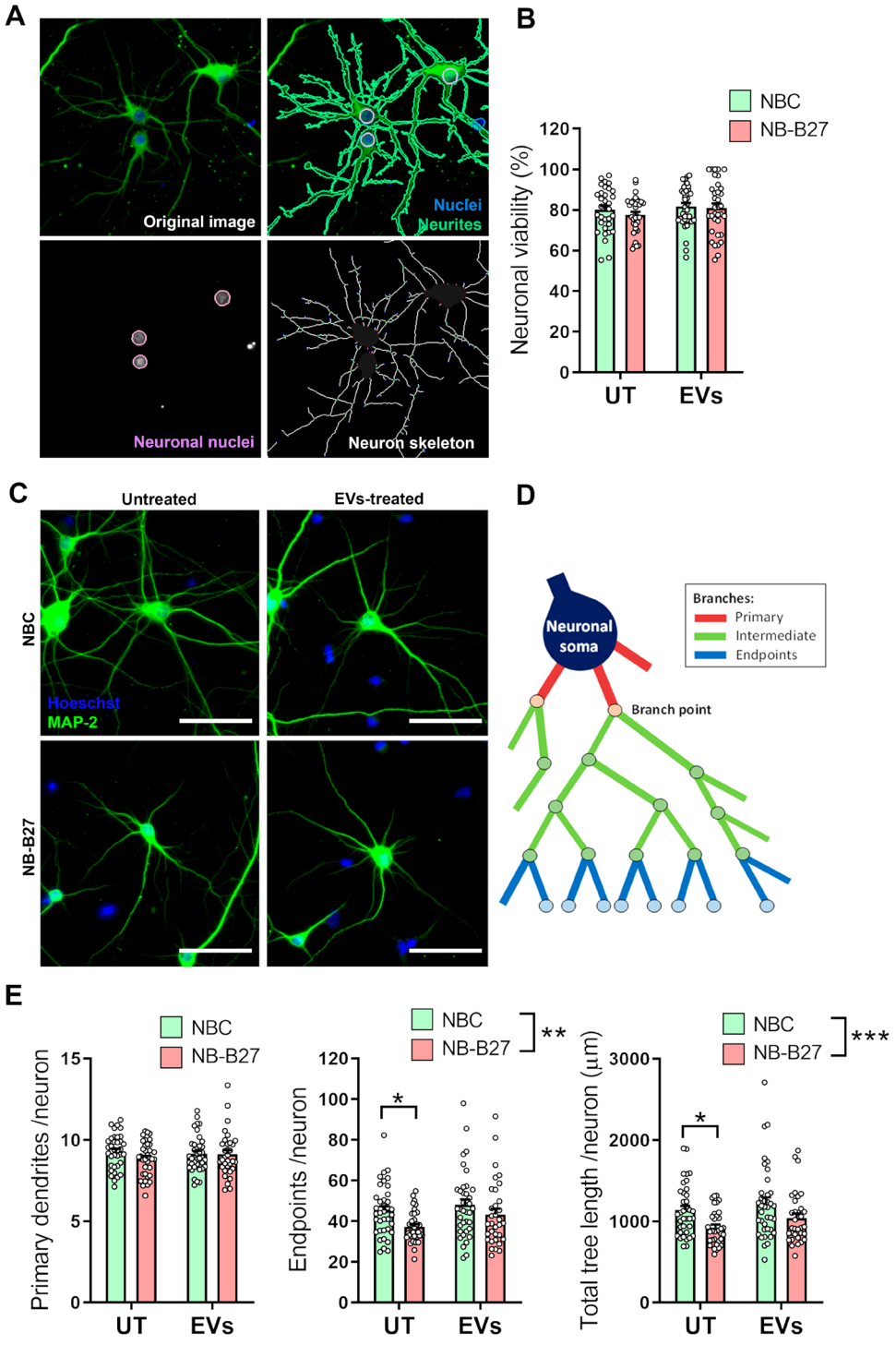

FIGURE 5 Neuron-derived EVs reverse neuronal morphological alterations of neurons under nutrient-deprivation conditions. Cultured neurons were either cultured in Neurobasal complete medium (NCB) or deprived from B27 supplement for 24 h (ND-B27). Just after the deprivation, neurons were treated with EVs for 24 h, and neuron arborization and viability were analysed (A) Immunocytochemistry for MAP-2 (green) was performed to visualize cultured neurons and Hoechst 33342 (blue) was used to visualize nuclei. Using CellProfiler software, neurons and nuclei were classified as individual objects. Neuronal nuclei were selected and classified into viable or apoptotic. Neuron morphology was analysed using the *MeasureObjectSkeleton* module. (B) Neuron viability analysis. (C) Representative images of neuron morphology in untreated or EVs-treated neurons, either cultured in NBC or in NB-B27 conditions. Scale bar of 50 µm. (D) Schematic representation of the different types of branches in a neuron. Endpoints represent the number of branch termini and total length the length of all skeleton segments per object. (E) Morphological assessment of neuronal cultures. The number of primary dendrites, endpoints, and total tree length were analysed. Values represent culture replicates of four independent neuronal cultures (mean ± SEM). Data was analysed by two-way ANOVA (*$P < 0.05$ vs. NBC).

specifically stronger over these two downstream effectors since EVs-treatment did not alter either phospho- or total TrkB levels in recipient neurons (Figure 4D), or either other plastic readout such as phospho-GluA1, phospho-ERK1/2, phospho-PKCα/β II, phospho-p70S6K and phospho-4E-BP1 (Figure S7).

We proved that the signalling effect was specific of neuron-derived EVs instead of other co-purified factors, as the treatment with NegCT for 24 h did not have any effect on recipient cortical neurons (Figure S6).

Altogether, these results suggest that EVs exert their plastic effect over Akt and RPS6 in recipient neurons, via vesicular TrkB.

3.3 | Spontaneous neural networks dynamics are not affected by EVs

Since the previous results showed an effect of EVs over synaptic spine density and excitatory synapses, we investigated whether EVs had a global modulatory function over neural networks dynamics. To do so, we measured spontaneous neuronal activity by analysing calcium fluorescent dynamics in both untreated and EVs-treated neuronal cultures for 24 h. We detected an average of 2400 individual cells (ROI) in both conditions. We extracted the fluorescent traces from the individual neurons in each culture and reconstructed their spike activity (Figure S8A1). Analysis of the spontaneous activity of neurons showed a tendency to decrease the average number of spikes by 22.44% in EVs-treated cultures compared to the untreated (UT) ones (Figure S8B), while spike patterns were unaltered, as shown by similar ISI distributions (Figure S8C).

To evaluate neuronal network dynamics, we determined collective activity events, which represent the fraction of neurons in the culture that are collectively activated in a small-time window, shaping a network burst (Figure S8A2). While the fraction of active network was unaltered upon EVs treatment (Figure S8D), there was a tendency for the network inter-burst interval to increase (by 41.36%), but it was not statistically significant (Figure S8E).

Hence, although EVs modulate spine number and molecular composition, this is not translated into the regulation of neuronal network dynamics.

3.4 | Neuron-derived EVs exert a trophic effect in recipient neurons

Lack of trophic support by BDNF in the brain areas is a common hallmark in pathological conditions (Miranda et al., 2019) such as many chronic neurodegenerative diseases (Seneff et al., 2011; Zuccato & Cattaneo, 2009). As we showed that EVs contain BDNF and its receptors, to gain further insight into EVs' function, we evaluated whether EVs could be trophic in nutrient deprivation conditions. Hence, B27 supplement was removed from cultured neurons for 24 h and, simultaneously, cells were treated with EVs. We analysed neuronal viability and morphology with CellProfiler software. Briefly, neuronal nuclei were selected, and data of intensity, granularity, texture, size, and shape were extracted per nuclei to classify them by machine learning into viable and apoptotic cells. Furthermore, neurons were individualized, and their skeleton was extracted to perform the arborization analysis (Figure 5A). Nutrient deprivation or EVs treatments during 24 h did not affect neuron viability (Figures 5B and S9). We then assessed neuron arborization complexity by classifying neurites into primary dendrites, intermediate branches, and termini branches (endpoints). The total tree length represents the length of all the branches in a neuron. (Figure 5C). We proved that mature neurons' morphology was altered with B27-deprived medium (NB-B27) during 24 h, as they showed fewer endpoints and reduced the total tree length compared to neurons maintained with the Neurobasal complete medium (NBC). In contrast, the primary dendrites remained unaltered after the deprivation. The presence of fewer endpoints indicates that after 24 h of nutrient deprivation, neuronal arborization is less abundant. Strikingly, we partially prevented this phenotype by the addition of neuron-derived EVs (Figure 5D,E), which supports the idea that EVs exert trophic support on neurons. The same effect was observed with SEC-isolated neuron-derived EVs (Figure S10). Moreover, similar effects were observed after treatment with a higher dose of EVs (Figure S11), suggesting we reached a plateau effect.

Importantly, the NegCT did not exert any trophic effect on nutrient-deprived neurons, confirming that the effect is mainly due to neuron-derived EVs (Figure S6).

Overall, these results suggest a crucial role of neuron-derived EVs in the regulation of neuronal morphology and hint at a potential neuroprotective role in neurodegeneration.

4 | DISCUSSION

Recent findings have exposed the role of EVs in the regulation of synaptic plasticity (reviewed in Graykowski et al., 2020). However, we are far from fully understanding how EVs, specifically the ones derived from neurons, are taking part in this intricate tuning. Here, we report that neuron-derived EVs contain synaptic proteins and are internalized via CME into neurons, where they promote spine formation while sparing spontaneous neuronal activity, probably by the transfer of active synaptic proteins, such as TrkB, that activate Akt and RPS6 intracellular signalling in the recipient neurons. Importantly, EVs were able to partially

restore neuronal morphological complexity under nutrient-deprivation conditions, demonstrating a key role of EVs in providing trophic support to neurons and highlighting their therapeutic potential for the treatment of neurodegenerative diseases.

We reported, using two different isolation methods (UC and SEC), that these EVs derived from cultured cortical neurons contain proteins that have largely been described to be mediators of synaptic plasticity. PSD-95 is a scaffolding protein that has an essential role in synapse maturation and allows fast excitatory postsynaptic potentials to occur (Kim et al., 2007). Although Fauré et al. (2006) reported that PSD-95 was not present in cortical EVs (Fauré et al., 2006) we could detect PSD95 in EVs, suggesting that it might potentiate the rapid formation of new synapses in the recipient neurons. Glutamate transporter, VGLUT-1, uptakes glutamate into the synaptic vesicles and is also essential for glutamatergic transmission (Saheki & Camilli, 2012). So far, VGLUT-1 has never been described to be a cargo in EVs. Here, we report the presence of VGLUT-1 in neuron-derived EVs, and we speculate that it could be an indicator of a retrograde signal via EVs. Indeed, the presence of both PSD-95 and VGLUT-1 in EVs could indicate that there is a release of EVs both at the anterograde and the retrograde level and those EVs contain the proteins naturally present at the synapses.

BDNF has a direct role in excitatory synaptic enhancement (Chapleau & Pozzo-Miller, 2012), so its presence in EVs strongly suggests its influence in synaptogenesis in recipient neurons. Although some studies in EVs isolated from plasma also reported the presence of BDNF (Chung et al., 2020; Saengsawang et al., 2017; Suire et al., 2017), we demonstrated that BDNF appears in EVs derived specifically from neurons. In addition, there is a strong link between the function of BDNF and the physiological levels of its receptors, TrkB and p75NTR (Zanin et al., 2019). The interaction of these two receptors requires their internalization into early endosomes, which could explain their presence in EVs. Indeed, Escudero et al. (2014) showed that p75NTR could evade the endo-lysosomal pathway in neurons and accumulates in multivesicular bodies, which are finally released into the extracellular medium as exosomes (Escudero et al., 2014). In line with our results, Sharma et al. (2019) described that EVs obtained from hiPSC-derived neural cultures contained TrkB as a cargo and these EVs reverted synaptogenesis deficit in a model of Rett syndrome (Sharma et al., 2019). Interestingly, it has been recently described that endocytic BDNF, TrkB and p75NTR continue signalling in the soma, dendrites and axons of cortical neurons to regulate dendritic arborization and spinogenesis (Moya-Alvarado et al., 2023), evidencing a new way of long-distance signalling of BDNF and its receptors. This finding raises the question of whether these BDNF-TrkB-p75NTR-loaded endosomes could, in fact, be internalized neuron-derived EVs.

Furthermore, we provided evidence that EVs are internalized by neurons not only at the soma but also at the dendrites and the dendritic spines. This result suggests a localized effect of neuron-derived EVs over synapses. We also showed that CME is a fundamental pathway by which EVs are taken up by neurons, although we cannot discard other minoritarian routes of internalization (Kwok et al., 2021).

Considering the neuron-derived EVs internalization by dendritic spines and their synaptic protein content, we studied their effect on synapses in recipient neurons. We found that primary cortical neurons treated with EVs presented an elevation in spine density and excitatory synapses. However, this elevation in the number of PSD-95/VGLUT-1 clusters was not accompanied by an increase in the area of the clusters or the intensity of these post and pre-synaptic markers, as a means of synaptic strength (Arellano et al., 2007; Béïque & Andrade, 2003; Pérez-Sisqués et al., 2021). Importantly, we proved that this effect was specific of EVs, as we observed the same effect with EVs isolated with an alternative method and we did not observe differences when neurons were treated with an EVs-free protein control or an EVs-free negative control containing co-purified factors from the medium (Auber et al., 2019).

In this line, we detected increased levels of PSD-95 in recipient neurons after the EVs treatment. This result is in concordance with Zhang et al. (2021), as they observed increased levels of PSD-95 in total lysates when neurons were treated with EVs derived from mature neurons but not from developing ones (Zhang et al., 2021). We did not detect changes in VGLUT-1 levels, which might indicate that EVs function is more localized at a post-synaptic level.

Strikingly, after EVs treatment, neurons presented elevated levels of phospho-Akt and phospho-RPS6, readouts of mTORC1 and mTORC2 kinases respectively (Canal et al., 2014). Akt is a downstream effector of phosphoinositide 3-kinase (PI3K), which is in turn activated by BDNF-activated TrkB receptor (Pradhan et al., 2019). Interestingly, Akt has been linked to synaptic structural modifications (Kim, 2022). Moreover, RPS6 is a component of the 40S ribosomal subunit, and its phosphorylation correlates with translational activation (Meyuhas, 2000). Long-term potentiation (LTP) induces the phosphorylation of RPS6 in postsynaptic neurons and is considered a crucial regulator of local protein synthesis in synapses (Pirbhoy et al., 2016), which could, in turn, promote spine formation. Importantly, we validated that this effect was exclusively due to EVs and not to other co-purified factors from the medium (Auber et al., 2019).

Moreover, we found that TrkB receptor was in its phosphorylated/active form in neuron-derived EVs. When TrkB activity was specifically blocked in EVs, neuron-derived EVs lost their ability to activate both Akt and RPS6. Therefore, our results position BDNF-TrkB-mediated signalling as the central mediator of the synaptic effect of neuron-derived EVs. EVs treatment did not increased TrkB phosphorylated levels in the recipient neurons, probably because the activated-TrkB signals directly to its downstream effectors in an endosome-mediated manner. Moreover, this result discards the possibility of being co-isolating the inhibitor along with the EVs. In line with our results, endosomes loaded with BDNF/TrkB also activated PI3K/Akt/mTOR pathway (Moya-Alvarado et al., 2023). Nevertheless, other molecules such as RNAs or lipids, or proteins such as mediators of the *Wnt* pathway (Lee et al., 2018), might contribute to the synaptic effect of EVs.

There is evidence that EVs can influence neuronal firing rate under pathological conditions (Prada et al., 2018; Sharma et al., 2019), but whether EVs could modulate neural networks in healthy cultured neurons was not yet assessed. Our results from the individual and collective spontaneous activity analysis showed that EVs-treatment did not significantly alter the individual neuronal spontaneous activity or network collective dynamics. This is consistent with the effects of chronic BDNF on healthy and Huntington's disease cultures, where BDNF modulates dendritic arborization but not network activity (García-Díaz Barriga et al., 2017). Indeed, BDNF has been shown to increase evoked responses (Jacobi et al., 2009), however, the effects on spontaneous neuronal activity are still not clear, as reviewed in Wang et al. (2022).

This is in line with our findings where we observed an increase in excitatory synapses after EVs treatment but no changes in the levels of PSD-95 in individual spines or in the area of PSD-95/VGLUT-1 clusters. As PSD-95 levels are correlated with neuronal activity (Roo et al., 2008; Sun & Turrigiano, 2011), our results suggest that EVs promote the formation of synaptic contacts without altering the synaptic strength of individual spines and therefore, do not change neuron spontaneous activity. These results evidence the potential role of EVs from healthy neurons to ameliorate synaptic deficiencies when added to stressed ones. In fact, EVs have been proposed to be a potential therapeutic tool in neurodegeneration (Rufino-Ramos et al., 2017; Zhang et al., 2015).

In the CNS, neurons require continuous trophic support for survival, and in many pathologies, such as stroke, traumatic brain injury, or chronic neurodegenerative diseases, trophic deprivation contributes to neuronal damage (Pang et al., 2014). In our neuronal cultures, although a 24 h nutrient deprivation did not induce neuron death, it significantly altered neuronal morphology, an effect that was partially prevented by EVs treatment. Although some studies described an effect of glial-derived EVs on neurite branching (Wang et al., 2011; Xin et al., 2017), nothing was known about neuron-derived EVs in nutrient-deprived neurons. Therefore, our results show a beneficial effect of neuronal EVs, suggesting their advantageous use to combat neurodegeneration in the near future (Rufino-Ramos et al., 2017; Zhang et al., 2015).

Overall, our results demonstrate that neuron-derived EVs contain synaptic proteins and trophic factors that exert trophic support to cortical neurons via their internalization through CME in soma, dendrites, and spines. Neuron-derived EVs promote spine formation and activate BDNF-TrkB signalling in recipient neurons and more importantly, EVs can restore neuron complexity deterioration induced by nutrient deprivation. Altogether, our results place neuron-derived EVs in the spotlight as neuromodulators to palliate both synaptic and morphological neuronal impairments.

AUTHOR CONTRIBUTIONS

Julia Solana-Balaguer: Conceptualization; data curation; formal analysis; funding acquisition; investigation; methodology; project administration; resources; software; supervision; validation; visualization; writing—original draft; writing—review & editing. **Genís Campoy-Campos**: Conceptualization; data curation; formal analysis; funding acquisition; investigation; methodology; project administration; resources; software; supervision; validation; visualization; writing—original draft; writing—review & editing. **Núria Martín-Flores**: Data curation; formal analysis; funding acquisition; investigation; methodology; project administration; software; supervision; validation; visualization; writing—original draft; writing—review & editing. **Leticia Pérez-Sisqués**: Conceptualization; data curation; formal analysis; funding acquisition; investigation; methodology; project administration; resources; software; supervision; validation; visualization; writing—original draft; writing—review & editing. **Laia Sitjà-Roqueta**: Conceptualization; data curation; formal analysis; funding acquisition; investigation; methodology; project administration; validation; visualization; writing—review & editing. **Melike Kucukerden**: Data curation; methodology; resources. **Ana Gámez-Valero**: Data curation; formal analysis; resources; validation; writing—review & editing. **Esther Pérez-Navarro**: Conceptualization; formal analysis; investigation; writing—review & editing. **Jordi Alberch**: Conceptualization; formal analysis; funding acquisition; investigation; resources; writing—review & editing. **Jordi Soriano**: Conceptualization; data curation; formal analysis; investigation; methodology; writing—original draft; writing—review & editing. **Mercè Masana**: Conceptualization; data curation; formal analysis; funding acquisition; investigation; methodology; project administration; resources; software; supervision; validation; visualization; writing—original draft; writing—review & editing. **Cristina Malagelada**: Conceptualization; data curation; formal analysis; funding acquisition; investigation; methodology; project administration; resources; software; supervision; validation; visualization; writing—original draft; writing—review & editing.

ACKNOWLEDGEMENTS

We thank J.M. Rebled (Centres Científics i Tecnològics, Universitat de Barcelona, CCiTUB) for help in electronic microscopy, Maria Calvo and Gemma Martín (Centres Científics i Tecnològics, Universitat de Barcelona, CCiTUB) for help in confocal microscopy and Amable Bernabé (Instituto de Ciencia de Materiales de Barcelona, ICMAB) for technical assistance from the NanoSight measurements. This work was supported by grants from Ministerio de Ciencia e Innovación /AEI/10.13039/501100011033/ and 'FEDER': SAF2017-88812-R and PID2020-119236RB-I00, from Cristina Malagelada; PID2020-119386RB-I00 from Jordi Alberch; PID2021-124896OA-I000, from Mercè Masana, PID2019-108842GB-C21, PID2019-106447RB-I00 from Esther Pérez-Navarro, PID2020-113953RB-I00 from Eulàlia Martí, by the Generalitat de Catalunya under the project 2017-SGR-1061 and by 'La Caixa' Foundation (ID 100010434) under agreement LCF/PR/HR19/52160007, from Jordi Soriano, and by Juan de la Cierva fellowship FJC2019-039633-I, from Ana Gámez-Valero. Julia Solana-Balaguer was supported

by an FPU grant from the Spanish Ministry of Science and Innovation (grant #FPU18/00194). Núria Martín-Flores was supported by a FPI grant from the Spanish Ministry of Science and Innovation (grant IBES-2015-072727). Genís Campoy-Campos was funded by a FI-2021 grant from the Agència de Gestió d'Ajuts Universitaris i de Recerca (AGAUR) (grant #FI-B-00378). Laia Sitjà-Roqueta was supported by an FPI grant PRE2020-092406 from the Spanish Ministry of Science and Innovation related to MDM-2017-0729 grant.

This research is part of NEUROPA. The NEUROPA Project has received funding from the European Union's Horizon 2020 Research and Innovation Program under Grant Agreement No. 863214 to Melike Kucukerden and Mercè Masana. Also, the project has been supported by María de Maeztu Unit of Excellent, Institute of Neurosciences, University of Barcelona, MDM-2017-0729, Ministry of Science, Innovation, and Universities.

CONFLICT OF INTEREST STATEMENT

All authors declare to have no conflict of interest.

REFERENCES

Arellano, J. I., Benavides-Piccione, R., Defelipe, J., & Yuste, R. (2007). Ultrastructure of dendritic spines: Correlation between synaptic and spine morphologies. Published online 2007. www.frontiersin.org

Auber, M., Fröhlich, D., Drechsel, O., Karaulanov, E., & Krämer-Albers, E. M. (2019). Serum-free media supplements carry miRNAs that co-purify with extracellular vesicles. *Journal of Extracellular Vesicles*, *8*(1), 1–10. https://doi.org/10.1080/20013078.2019.1656042

Béïque, J. C., & Andrade, R. (2003). PSD-95 regulates synaptic transmission and plasticity in rat cerebral cortex. *The Journal of Physiology*, *546*(Pt 3), 859–867. https://doi.org/10.1113/JPHYSIOL.2002.031369

Boyer, M. J., Kimura, Y., Akiyama, T., Baggett, A. Y., Preston, K. J., Scalia, R., Eguchi, S., & Rizzo, V. (2020). Endothelial cell-derived extracellular vesicles alter vascular smooth muscle cell phenotype through high-mobility group box proteins. *Journal of Extracellular Vesicles*, *9*(1), 1781427. https://doi.org/10.1080/20013078.2020.1781427

Budnik, V., Ruiz-Cañada, C., & Wendler, F. (2016). Extracellular vesicles round off communication in the nervous system. *Nature Reviews Neuroscience*, *17*(3), 160. https://doi.org/10.1038/NRN.2015.29

Canal, M., Romaní-Aumedes, J., Martín-Flores, N., Pérez-Fernández, V., & Malagelada, C. (2014). RTP801/REDD1: A stress coping regulator that turns into a troublemaker in neurodegenerative disorders. *Frontiers in Cellular Neuroscience*, *8*, (Oct), 313. https://doi.org/10.3389/FNCEL.2014.00313/BIBTEX

Carpenter, A. E., Jones, T. R., Lamprecht, M. R., Clarke, C., Kang, I., Friman, O., Guertin, D. A., Chang, J., Lindquist, R. A., Moffat, J., Golland, P., & Sabatini, D. M. (2006). *Genome Biology*, *7*(10), R100. https://doi.org/10.1186/gb-2006-7-10-r100

Cazorla, M., Prémont, J., Mann, A., Girard, N., Kellendonk, C., & Rognan, D. (2011). Identification of a low-molecular weight TrkB antagonist with anxiolytic and antidepressant activity in mice. *Journal of Clinical Investigation*, *121*(5), 1846. https://doi.org/10.1172/JCI43992

Chapleau, C. A., & Pozzo-Miller, L. (2012). Divergent roles of p75NTR and Trk receptors in BDNF's effects on dendritic spine density and morphology. *Neural Plasticity*, *2012*, 1–19. https://doi.org/10.1155/2012/578057

Chivet, M., Javalet, C., Laulagnier, K., Blot, B., Hemming, F. J., & Sadoul, R. (2014). Exosomes secreted by cortical neurons upon glutamatergic synapse activation specifically interact with neurons. *Journal of Extracellular Vesicles*, *3*(1), 24722. https://doi.org/10.3402/JEV.V3.24722

Chung, C. C., Huang, P. H., Chan, L., Chen, J. H., Chien, L. N., & Hong, C. T. (2020). Plasma exosomal brain-derived neurotrophic factor correlated with the postural instability and gait disturbance-related motor symptoms in patients with Parkinson's disease. *Diagnostics*, *10*(9), 684. https://doi.org/10.3390/DIAGNOSTICS10090684

Chuo, S. T. Y., Chien, J. C. Y., & Lai, C. P. K. (2018). Imaging extracellular vesicles: Current and emerging methods. *Journal of Biomedical Science*, *25*(1), 1–10. https://doi.org/10.1186/S12929-018-0494-5/FIGURES/3

Collot, M., Ashokkumar, P., Anton, H., Boutant, E., Faklaris, O., Galli, T., Mély, Y., Danglot, L., & Klymchenko, A. S. (2019). MemBright: A family of fluorescent membrane probes for advanced cellular imaging and neuroscience. *Cell Chemical Biology*, *26*(4), 600–614.e7. https://doi.org/10.1016/j.chembiol.2019.01.009

Danzer, K. M., Kranich, L. R., Ruf, W. P., Cagsal-Getkin, O., Winslow, A. R., Zhu, L., Vanderburg, C. R., & McLean, P. J. (2012). Exosomal cell-to-cell transmission of alpha synuclein oligomers. *Molecular Neurodegeneration*, *7*(1), 1–18. https://doi.org/10.1186/1750-1326-7-42

Danzer, K. M., Kranich, L. R., Ruf, W. P., Cagsal-Getkin, O., Winslow, A. R., Zhu, L., Vanderburg, C. R., & McLean, P. J. (2012). Exosomal cell-to-cell transmission of alpha synuclein oligomers. *Molecular Neurodegeneration*, *7*(1), https://doi.org/10.1186/1750-1326-7-42

Emmanouilidou, E., Melachroinou, K., Roumeliotis, T., Garbis, S. D., Ntzouni, M., Margaritis, L. H., Stefanis, L., & Vekrellis, K. (2010). Cell-produced α-synuclein is secreted in a calcium-dependent manner by exosomes and impacts neuronal survival. *The Journal of Neuroscience*, *30*(20), 6838–6851. https://doi.org/10.1523/jneurosci.5699-09.2010

Escudero, C., Lazo, O., Galleguillos, C., Parraguez, J., Lopez-Verrilli, M., Cabeza, C., Leon, L., Saeed, U., Retamal, C., Gonzalez, A., Marzolo, M., Carter, B., Court, F., & Bronfman, F. (2014). p75 neurotrophin receptor evades the endolysosomal route, favouring multivesicular bodies specialised for exosomal release in neuronal cells. *Journal of Cell Science*, *127*(9), 1966–1979. https://doi.org/10.1242/jcs.141754

Fahnestock, M., & Nicolini, C. (2015). Bridging the gap between genes and behavior: Brain-derived neurotrophic factor and the mTOR pathway in idiopathic autism. *Autism Open Access*, *5*(2), 1–10. https://doi.org/10.4172/2165-7890.1000143

Fauré, J., Lachenal, G., Court, M., Hirrlinger, J., Chatellard-Causse, C., Blot, B., Grange, J., Schoehn, G., Goldberg, Y., Boyer, V., Kirchhoff, F., Raposo, G., Garin, J., & Sadoul, R. (2006). Exosomes are released by cultured cortical neurones. *Molecular and Cellular Neuroscience*, *31*(4), 642–648. https://doi.org/10.1016/j.mcn.2005.12.003

Fernández-García, S., Orlandi, J. G., García-Díaz Barriga, G.-D., Rodríguez, M. J., Masana, M., Soriano, J., & Alberch, J. (2020). Deficits in coordinated neuronal activity and network topology are striatal hallmarks in Huntington's disease. *BMC Biology*, *18*(1), 1–16. https://doi.org/10.1186/s12915-020-00794-4

Francia, V., Reker-Smit, C., Boel, G., & Salvati, A. (2019). Limits and challenges in using transport inhibitors to characterize how nano-sized drug carriers enter cells. *Nanomedicine (London)*, *14*(12), 1533–1549. https://doi.org/10.2217/NNM-2018-0446

Frühbeis, C., Fröhlich, D., Kuo, W. P., & Krämer-Albers, E. M. (2013). Extracellular vesicles as mediators of neuron-glia communication. *Frontiers in Cellular Neuroscience*, *7*, 1–6. https://doi.org/10.3389/FNCEL.2013.00182

Frühbeis, C., Kuo-Elsner, W. P., Müller, C., Barth, K., Peris, L., Tenzer, S., Möbius, W., Werner, H. B., Nave, K.-A., Fröhlich, D., & Krämer-Albers, E.-M. (2020). Oligodendrocytes support axonal transport and maintenance via exosome secretion. *PLOS Biology*, *18*(12), e3000621. https://doi.org/10.1371/journal.pbio.3000621

Gámez-Valero, A., Monguió-Tortajada, M., Carreras-Planella, L., Franquesa, M., Beyer, K., & Borràs, F. E. (2016). Size-exclusion chromatography-based isolation minimally alters extracellular vesicles' characteristics compared to precipitating agents. *Scientific Reports*, *6*, 33641. https://doi.org/10.1038/SREP33641

García-Díaz Barriga, G., Giralt, A., Anglada-Huguet, M., Gaja-Capdevila, N., Orlandi, J. G., Soriano, J., Canals, J.-M., & Alberch, J. (2017). 7,8-dihydroxyflavone ameliorates cognitive and motor deficits in a Huntington's disease mouse model through specific activation of the PLCγ1 pathway. *Human Molecular Genetics*, *26*(16), 3144–3160. https://doi.org/10.1093/hmg/ddx198

Gassama, Y., & Favereaux, A. (2021). Emerging roles of extracellular vesicles in the central nervous system: Physiology, pathology, and therapeutic perspectives. *Front Cell Neuroscience*, *15*, 7. https://doi.org/10.3389/FNCEL.2021.626043/BIBTEX

Gould, S. J., & Raposo, G. (2013). As we wait: Coping with an imperfect nomenclature for extracellular vesicles. *Journal of Extracellular Vesicles*, *2*(1), 1–3. https://doi.org/10.3402/JEV.V2I0.20389

Graykowski, D. R., Wang, Y. Z., Upadhyay, A., & Savas, J. N. (2020). The dichotomous role of extracellular vesicles in the central nervous system. *iScience*, *23*(9), 1–15. https://doi.org/10.1016/J.ISCI.2020.101456

Holm, M. M., Kaiser, J., & Schwab, M. E. (2018). Extracellular vesicles: Multimodal envoys in neural maintenance and repair. *Trends in Neuroscience (Tins)*, *41*(6), 360–372. https://doi.org/10.1016/j.tins.2018.03.006

Horch, H. W., & Katz, L. C. (2002). BDNF release from single cells elicits local dendritic growth in nearby neurons. *Nature Neuroscience*, *5*(11), 1177–1184. https://doi.org/10.1038/nn927

Jacobi, S., Soriano, J., Segal, M., & Moses, E. (2009). BDNF and NT-3 increase excitatory input connectivity in rat hippocampal cultures. *European Journal of Neuroscience*, *30*(6), 998–1010. https://doi.org/10.1111/J.1460-9568.2009.06891.X

Jones, T. R., Carpenter, A. E., Lamprecht, M. R., Moffat, J., Silver, S. J., Grenier, J. K., Castoreno, A. B., Eggert, U. S., Root, D. E., Golland, P., & Sabatini, D. M. (2009). Scoring diverse cellular morphologies in image-based screens with iterative feedback and machine learning. *Proceedings of the National Academy of Sciences*, *106*(6), 1826–1831. https://doi.org/10.1073/pnas.0808843106

Jones, T. R., Kang, I. H., Wheeler, D. B., Lindquist, R. A., Papallo, A., Sabatini, D. M., Golland, P., & Carpenter, A. E. (2008). CellProfiler analyst: Data exploration and analysis software for complex image-based screens. *BMC Bioinformatics [Electronic Resource]*, *9*(1), 1–16. https://doi.org/10.1186/1471-2105-9-482

Jung, M. K., & Mun, J. Y. (2018). Sample preparation and imaging of exosomes by transmission electron microscopy. *Journal of visualized experiments: JoVE*, *2018*(131), 56482. https://doi.org/10.3791/56482

Kim, M. J., Futai, K., Jo, J., Hayashi, Y., Cho, K., & Sheng, M. (2007). Synaptic accumulation of PSD-95 and synaptic function regulated by phosphorylation of serine-295 of PSD-95. *Neuron*, *56*(3), 488–502. https://doi.org/10.1016/j.neuron.2007.09.007

Kim, Y. J. (2022). Activity-induced synaptic structural modifications by Akt. *Biochemical and Biophysical Research Communications*, *621*, 94–100. https://doi.org/10.1016/J.BBRC.2022.06.093

Korkut, C., Li, Y., Koles, K., Brewer, C., Ashley, J., Yoshihara, M., & Budnik, V. (2013). Regulation of postsynaptic retrograde signaling by presynaptic exosome release. *Neuron*, *77*(6), 1039–1046. https://doi.org/10.1016/j.neuron.2013.01.013

Kwok, Z. H., Wang, C., & Jin, Y. (2021). Extracellular vesicle transportation and uptake by recipient cells: A critical process to regulate human diseases. *Processes 2021*, *9*(2), 273. https://doi.org/10.3390/PR9020273

Lee, S. H., Shin, S. M., Zhong, P., Kim, H.-T., Kim, D.-I., Kim, J. M., Heo, W. D., Kim, D.-W., Yeo, C.-Y., Kim, C.-H., & Liu, Q. (2018). Reciprocal control of excitatory synapse numbers by Wnt and Wnt inhibitor PRR7 secreted on exosomes. *Nature Communications*, *9*(1), 1–15. https://doi.org/10.1038/s41467-018-05858-2

Lindholm, D., Hengerer, B., & Ċastrén, E. (1993). In Vitro and in vivo methods for evaluating actions of cytokines on nerve growth factor production in central nervous system. *Methods in Neurosciences*, *17*(PB), 37–60. https://doi.org/10.1016/S1043-9471(13)70008-9

Martín-Flores, N., Romaní-Aumedes, J., Rué, L., Canal, M., Sanders, P., Straccia, M., Allen, N. D., Alberch, J., Canals, J. M., Pérez-Navarro, E., & Malagelada, C. (2015). RTP801 is involved in mutant huntingtin-induced cell death. *Molecular Neurobiology*, *53*(5), 2857–2868. https://doi.org/10.1007/s12035-015-9166-6

Meyuhas, O. (2000). Synthesis of the translational apparatus is regulated at the translational level. *European Journal of Biochemistry*, *267*(21), 6321–6330. https://doi.org/10.1046/J.1432-1327.2000.01719.X

Miranda, M., Morici, J. F., Zanoni, M. B., & Bekinschtein, P. (2019). Brain-derived neurotrophic factor: A key molecule for memory in the healthy and the pathological brain. *Frontiers in Cellular Neuroscience*, *13*, 363. https://doi.org/10.3389/FNCEL.2019.00363/BIBTEX

Monguió-Tortajada, M., Morón-Font, M., Gámez-Valero, A., Carreras-Planella, L., Borràs, F. E., & Franquesa, M. (2019). Extracellular-vesicle isolation from different biological fluids by size-exclusion chromatography. *Current Protocols in Stem Cell Biology*, *49*(1), e82. https://doi.org/10.1002/CPSC.82

Montalà-Flaquer, M., López-León, C. F., Tornero, D., Houben, A. M., Fardet, T., Monceau, P., Bottani, S., & Soriano, J. (2022). Rich dynamics and functional organization on topographically designed neuronal networks in vitro. *IScience*, *25*(12), 105680. https://doi.org/10.1016/j.isci.2022.105680

Moya-Alvarado, G., Tiburcio-Felix, R., Ibáñez, M. R., Aguirre-Soto, A. A., Guerra, M. V., Wu, C., Mobley, W. C., Perlson, E., & Bronfman, F. C. (2023). BDNF/TrkB signaling endosomes in axons coordinate CREB/mTOR activation and protein synthesis in the cell body to induce dendritic growth in cortical neurons. *ELife*, *12*, e77455. CLOCKSS. https://doi.org/10.7554/elife.77455

Norman, M., Ter-Ovanesyan, D., Trieu, W., Lazarovits, R., Kowal, E. J. K., Lee, J. H., Chen-Plotkin, A. S., Regev, A., Church, G. M., & Walt, D. R. (2021). L1CAM is not associated with extracellular vesicles in human cerebrospinal fluid or plasma. *Nature Methods*, *18*(6), 631–634. https://doi.org/10.1038/s41592-021-01174-8

Orlandi, J. G., Fernández-García, S., Comella-Bolla, A., Masana, M., Barriga, G. G.-D., Yaghoubi, M., Kipp, A., Canals, J. M., Colicos, M. A., Davidsen, J., Alberch, J., & Soriano, J. (2017). NETCAL: An interactive platform for large-scale, NETwork and population dynamics analysis of CALcium imaging recordings(7.0.0 Open Beta) [Computer software]. Zenodo. https://doi.org/10.5281/ZENODO.1119026

Pang, T., Sun, L. X., Wang, T., Jiang, Z. Z., Liao, H., & Zhang, L. Y. (2014). Telmisartan protects central neurons against nutrient deprivation-induced apoptosis in vitro through activation of PPARγ and the Akt/GSK-3β pathway. *Acta Pharmacologica Sinica*, *35*(6), 727–737. https://doi.org/10.1038/APS.2013.199

Pastuzyn, E. D., Day, C. E., Kearns, R. B., Kyrke-Smith, M., Taibi, A. V., McCormick, J., Yoder, N., Belnap, D. M., Erlendsson, S., Morado, D. R., Briggs, J. A. G., Feschotte, C., & Shepherd, J. D. (2018). The neuronal gene arc encodes a repurposed retrotransposon gag protein that mediates intercellular RNA transfer. *Cell*, *172*(1–2), 275–288.e18. https://doi.org/10.1016/j.cell.2017.12.024

Pérez-Sisqués, L., Martín-Flores, N., Masana, M., Solana-Balaguer, J., Llobet, A., Romaní-Aumedes, J., Canal, M., Campoy-Campos, G., García-García, E., Sánchez-Fernández, N., Fernández-García, S., Gilbert, J. P., Rodríguez, M. J., Man, H.-Y., Feinstein, E., Williamson, D. L., Soto, D., Gasull, X., Alberch, J., & Malagelada, C. (2021). RTP801 regulates motor cortex synaptic transmission and learning. *Experimental Neurology*, *342*, 113755. https://doi.org/10.1016/j.expneurol.2021.113755

Pfrieger, F. W., & Barres, B. A. (1997). Synaptic efficacy enhanced by glial cells in vitro. *Science (1979)*, *277*(5332), 1684–1687. https://doi.org/10.1126/SCIENCE.277.5332.1684

Pirbhoy, P. S., Farris, S., & Steward, O. (2016). Synaptic activation of ribosomal protein S6 phosphorylation occurs locally in activated dendritic domains. *Learning & Memory*, *23*(6), 255–269. https://doi.org/10.1101/LM.041947.116

Prada, I., Gabrielli, M., Turola, E., Iorio, A., D'Arrigo, G., Parolisi, R., De Luca, M., Pacifici, M., Bastoni, M., Lombardi, M., Legname, G., Cojoc, D., Buffo, A., Furlan, R., Peruzzi, F., & Verderio, C. (2018). Glia-to-neuron transfer of miRNAs via extracellular vesicles: A new mechanism underlying inflammation-induced synaptic alterations. *Acta Neuropathologica*, *135*(4), 529–550. https://doi.org/10.1007/s00401-017-1803-x

Pradhan, J., Noakes, P. G., & Bellingham, M. C. (2019). The role of altered BDNF/TrkB signaling in amyotrophic lateral sclerosis. *Frontiers in Cellular Neuroscience*, *13*, 368. https://doi.org/10.3389/FNCEL.2019.00368/BIBTEX

Preta, G., Cronin, J. G., & Sheldon, I. M. (2015). Dynasore - Not just a dynamin inhibitor. *Cell Communication and Signaling*, *13*(1), 1–7. https://doi.org/10.1186/S12964-015-0102-1/TABLES/1

Quek, C., & Hill, A. F. (2017). The role of extracellular vesicles in neurodegenerative diseases. *Biochemical and Biophysical Research Communications*, *483*(4), 1178–1186. https://doi.org/10.1016/J.BBRC.2016.09.090

Rajendran, L., Bali, J., Barr, M. M., Court, F. A., Krämer-Albers, E.-M., Picou, F., Raposo, G., van der Vos, K. E., van Niel, G., Wang, J., & Breakefield, X. O. (2014). Emerging roles of extracellular vesicles in the nervous system. *The Journal of Neuroscience*, *34*(46), 15482–15489. https://doi.org/10.1523/jneurosci.3258-14.2014

Rajendran, L., Honsho, M., Zahn, T. R., Keller, P., Geiger, K. D., Verkade, P., & Simons, K. (2006). Alzheimer's disease β-amyloid peptides are released in association with exosomes. *Proceedings of the National Academy of Sciences*, *103*(30), 11172–11177. https://doi.org/10.1073/pnas.0603838103

Roo de, M., Klauser, P., Mendez, P., Poglia, L., & Muller, D. (2008). Activity-dependent PSD formation and stabilization of newly formed spines in hippocampal slice cultures. *Cerebral Cortex*, *18*(1), 151–161. https://doi.org/10.1093/CERCOR/BHM041

Rufino-Ramos, D., Albuquerque, P. R., Carmona, V., Perfeito, R., Nobre, R. J., & Pereira de Almeida, L. (2017). Extracellular vesicles: Novel promising delivery systems for therapy of brain diseases. *Journal of Controlled Release*, *262*, 247–258. https://doi.org/10.1016/J.JCONREL.2017.07.001

Saengsawang, W., Kongoun, S., & Chanda, M. (2017). Exercise increases brain-derived neurotrophic factor in serum exosomes. *The FASEB Journal*, *31*, 839.5–839.5. https://doi.org/10.1096/FASEBJ.31.1_SUPPLEMENT.839.5

Saheki, Y., & Camilli, de P. (2012). Synaptic vesicle endocytosis. *Cold Spring Harbor Perspectives in Biology*, *4*(9), 1–30. https://doi.org/10.1101/CSHPERSPECT.A005645

Schnatz, A., Müller, C., Brahmer, A., & Krämer-Albers, E. M. (2021). Extracellular vesicles in neural cell interaction and CNS homeostasis. *FASEB Bioadvances*, *3*(8), 577–592. https://doi.org/10.1096/FBA.2021-00035

Seneff, S., Wainwright, G., & Mascitelli, L. (2011). Nutrition and Alzheimer's disease: The detrimental role of a high carbohydrate diet. *European Journal of Internal Medicine*, *22*(2), 134–140. https://doi.org/10.1016/J.EJIM.2010.12.017

Sharma, P., Mesci, P., Carromeu, C., McClatchy, D. R., Schiapparelli, L., Yates, J. R., Muotri, A. R., & Cline, H. T. (2019). Exosomes regulate neurogenesis and circuit assembly. *Proceedings of the National Academy of Sciences*, *116*(32), 16086–16094. https://doi.org/10.1073/pnas.1902513116

Stirling, D. R., Carpenter, A. E., & Cimini, B. A. (2021). CellProfiler Analyst 3.0: Accessible data exploration and machine learning for image analysis. *Bioinformatics*, *37*(21), 3992–3994. https://doi.org/10.1093/BIOINFORMATICS/BTAB634

Stirling, D. R., Swain-Bowden, M. J., Lucas, A. M., Carpenter, A. E., Cimini, B. A., & Goodman, A. (2021). CellProfiler 4: Improvements in speed, utility and usability. *BMC Bioinformatics [Electronic Resource]*, *22*(1), 1–11. https://doi.org/10.1186/S12859-021-04344-9/FIGURES/6

Suire, C. N., Eitan, E., Shaffer, N. C., Tian, Q., Studenski, S., Mattson, M. P., & Kapogiannis, D. (2017). Walking speed decline in older adults is associated with elevated pro-BDNF in plasma extracellular vesicles. *Experimental Gerontology*, *98*, 209–216. https://doi.org/10.1016/j.exger.2017.08.024

Sun, Q., & Turrigiano, G. G. (2011). PSD-95 and PSD-93 play critical but distinct roles in synaptic scaling up and down. *Journal of Neuroscience*, *31*(18), 6800–6808. https://doi.org/10.1523/JNEUROSCI.5616-10.2011

Takeuchi, T. (2021). Pathogenic and protective roles of extracellular vesicles in neurodegenerative diseases. *The Journal of Biochemistry*, *169*(2), 181–186. https://doi.org/10.1093/JB/MVAA131

Théry, C., Witwer, K. W., Aikawa, E., Alcaraz, M. J., Anderson, J. D., Andriantsitohaina, R., Antoniou, A., Arab, T., Archer, F., Atkin-Smith, G. K., Ayre, D. C., Bach, J. M., Bachurski, D., Baharvand, H., Balaj, L., Baldacchino, S., Bauer, N. N., Baxter, A. A., Bebawy, M., … Zuba-Surma, E. K. (2018). Minimal information for studies of extracellular vesicles 2018 (MISEV2018): A position statement of the International Society for Extracellular Vesicles and update of the MISEV2014 guidelines. *Journal of extracellular vesicles*, *7*(1), 1535750. https://doi.org/10.1080/20013078.2018.1535750

Van Niel, G., D'Angelo, G., & Raposo, G. (2018). Shedding light on the cell biology of extracellular vesicles. *Nature Reviews Molecular Cell Biology*, *19*(4), 213–228. https://doi.org/10.1038/NRM.2017.125

Wang, C. S., Kavalali, E. T., & Monteggia, L. M. (2022). BDNF signaling in context: From synaptic regulation to psychiatric disorders. *Cell*, *185*(1), 62–76. https://doi.org/10.1016/J.CELL.2021.12.003

Wang, S., Cesca, F., Loers, G., Schweizer, M., Buck, F., Benfenati, F., Schachner, M., & Kleene, R. (2011). Synapsin I is an oligomannose-carrying glycoprotein, acts as an oligomannose-binding lectin, and promotes neurite outgrowth and neuronal survival when released via glia-derived exosomes. *The Journal of Neuroscience*, *31*(20), 7275–7290. https://doi.org/10.1523/jneurosci.6476-10.2011

Wang, Y., Balaji, V., Kaniyappan, S., Krüger, L., Irsen, S., Tepper, K., Chandupatla, R., Maetzler, W., Schneider, A., Mandelkow, E., & Mandelkow, E.-M. (2017). The release and trans-synaptic transmission of Tau via exosomes. *Molecular Neurodegeneration*, *12*(1), 1–25. https://doi.org/10.1186/s13024-016-0143-y

Xia, X., Wang, Y., Qin, Y., Zhao, S., & Zheng, J. C. (2022). Exosome: A novel neurotransmission modulator or non-canonical neurotransmitter? *Ageing Research Reviews*, *74*, 101558. https://doi.org/10.1016/J.ARR.2021.101558

Xin, H., Wang, F., Li, Y., Lu, Q.-E., Cheung, W. L., Zhang, Y., Zhang, Z. G., & Chopp, M. (2017). Secondary release of exosomes from astrocytes contributes to the increase in neural plasticity and improvement of functional recovery after stroke in rats treated with exosomes harvested from microRNA 133b-overexpressing multipotent mesenchymal stromal cells. *Cell Transplantation*, *26*(2), 243–257. https://doi.org/10.3727/096368916x693031

Xu, R., Greening, D. W., Zhu, H. J., Takahashi, N., & Simpson, R. J. (2016). Extracellular vesicle isolation and characterization: Toward clinical application. *Journal of Clinical Investigation*, *126*(4), 1152. https://doi.org/10.1172/JCI81129

Yáñez-Mó, M., Siljander, P. R.-M., Andreu, Z., Zavec, B., Borràs, F. E., Buzas, E. I., Buzas, K., Casal, E., Cappello, F., Carvalho, J., Colás, E., Cordeiro-da Silva, A., Fais, S., Falcon-Perez, J. M., Ghobrial, I. M., Giebel, B., Gimona, M., Graner, M., Gursel, I., … de Wever, O. (2015). Biological properties of extracellular vesicles and their physiological functions. *Journal of Extracellular Vesicles*, *4*(1), 27066. https://doi.org/10.3402/jev.v4.27066

Zagrebelsky, M., Tacke, C., & Korte, M. (2020). BDNF signaling during the lifetime of dendritic spines. *Cell and Tissue Research*, *382*(1), 185. https://doi.org/10.1007/S00441-020-03226-5

Zanin, J. P., Montroull, L. E., Volosin, M., & Friedman, W. J. (2019). The p75 neurotrophin receptor facilitates TrkB signaling and function in rat hippocampal neurons. *Frontiers in Cellular Neuroscience*, *13*, 485. https://doi.org/10.3389/FNCEL.2019.00485

Zhang, L., Lin, T. v., Yuan, Q., Sadoul, R., Lam, T. K. T., & Bordey, A. (2021). Small extracellular vesicles control dendritic spine development through regulation of HDAC2 signaling. *Journal of Neuroscience*, *41*(17), 3799–3807. https://doi.org/10.1523/JNEUROSCI.0766-20.2021

Zhang, Y., Chopp, M., Meng, Y., Katakowski, M., Xin, H., Mahmood, A., & Xiong, Y. (2015). Effect of exosomes derived from multipluripotent mesenchymal stromal cells on functional recovery and neurovascular plasticity in rats after traumatic brain injury. *Journal of Neurosurgery*, *122*(4), 856–867. https://doi.org/10.3171/2014.11.jns14770

Zuccato, C., & Cattaneo, E. (2009). Brain-derived neurotrophic factor in neurodegenerative diseases. *Nature Reviews Neurology*, *5*(6), 311–322. https://doi.org/10.1038/NRNEUROL.2009.54

SUPPORTING INFORMATION

Additional supporting information can be found online in the Supporting Information section at the end of this article.

How to cite this article: Solana-Balaguer, J., Campoy-Campos, G., Martín-Flores, N., Pérez-Sisqués, L., Sitjà-Roqueta, L., Kucukerden, M., Gámez-Valero, A., Coll-Manzano, A., Martí, E., Pérez-Navarro, E., Alberch, J., Soriano, J., Masana, M., & Malagelada, C. (2023). Neuron-derived extracellular vesicles contain synaptic proteins, promote spine formation, activate TrkB-mediated signalling and preserve neuronal complexity. *Journal of Extracellular Vesicles*, *12,* e12355. https://doi.org/10.1002/jev2.12355

Supplementary Figure 1

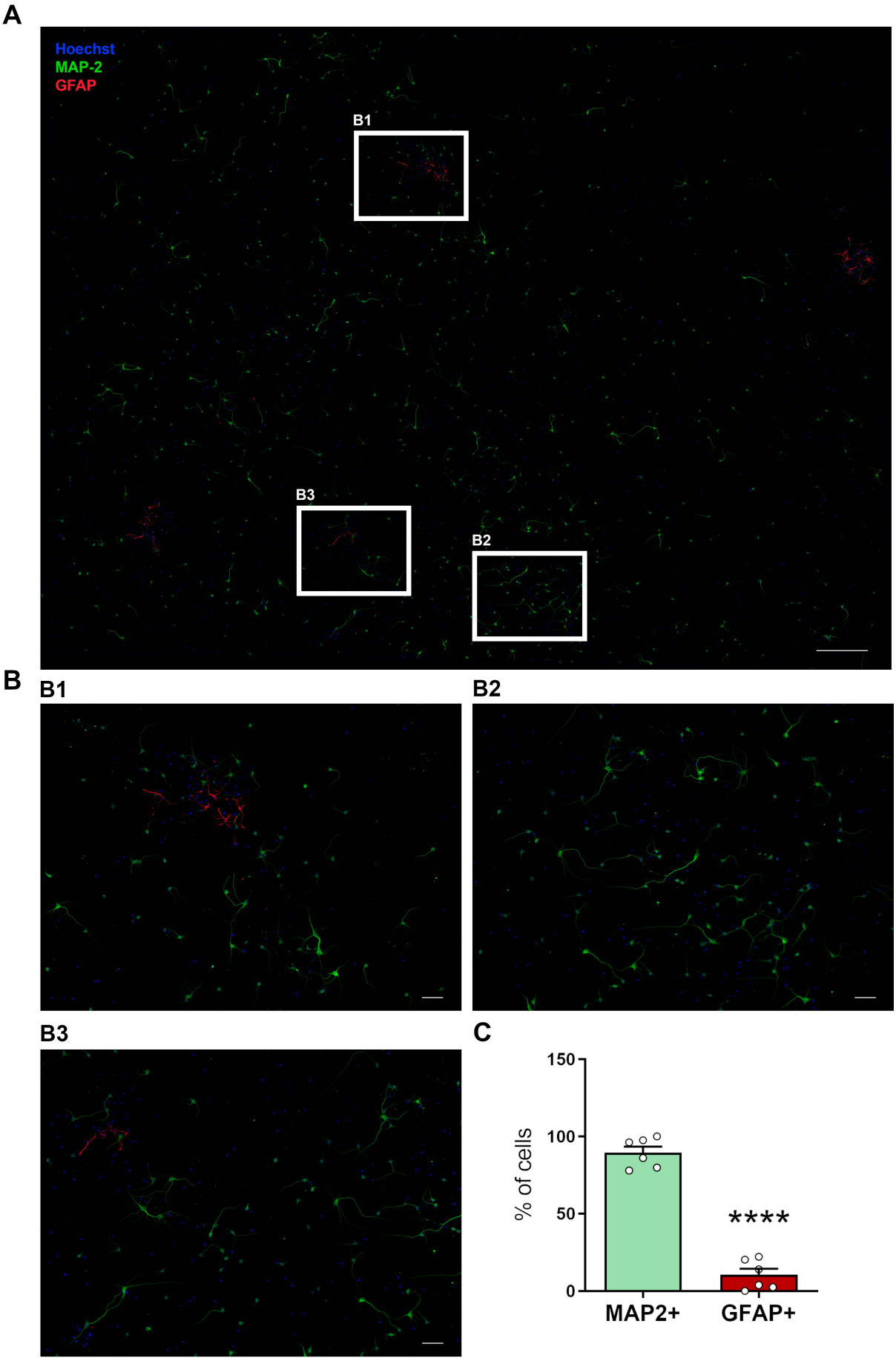

Supplementary Figure 2

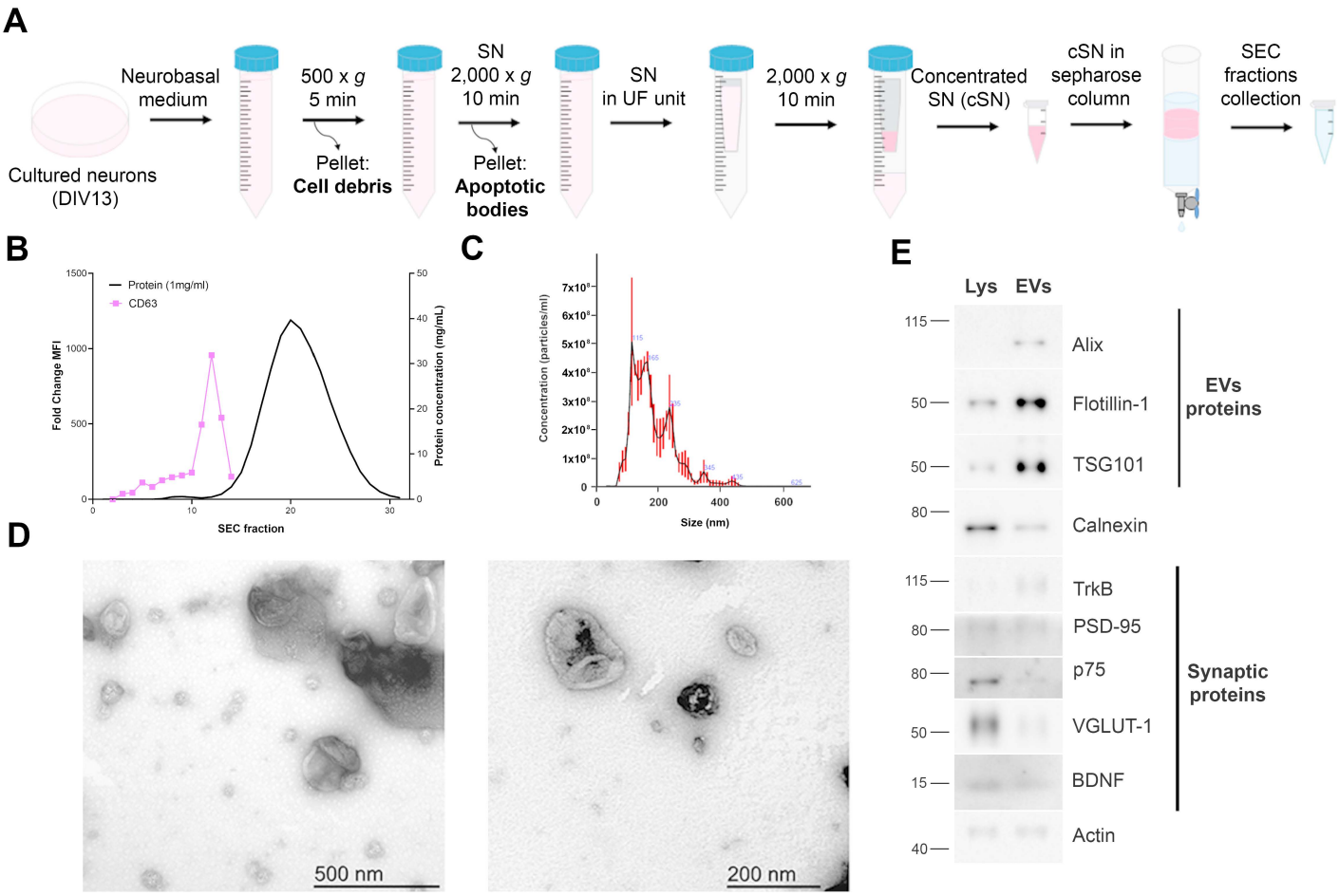

Supplementary Figure 3

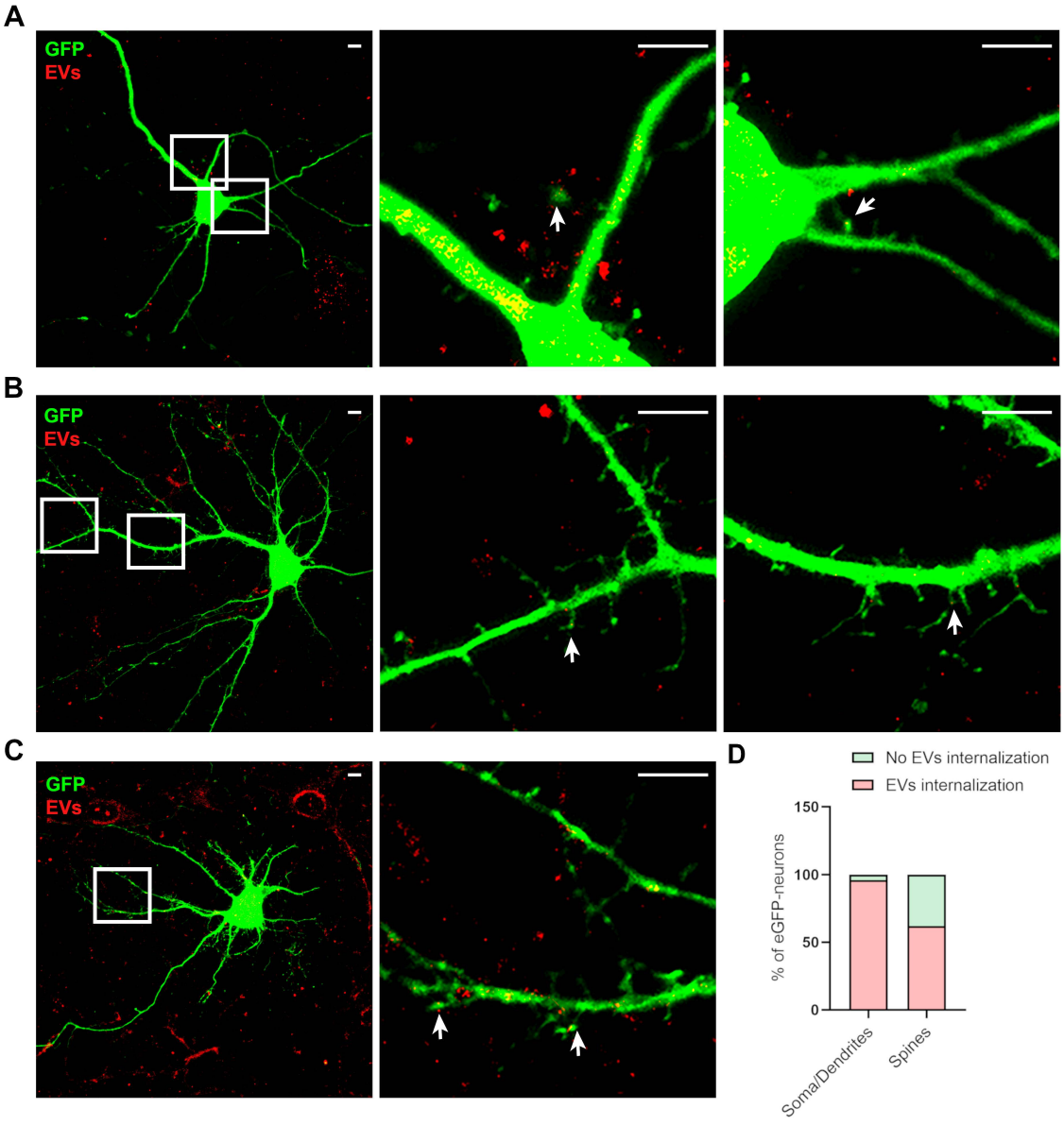

Supplementary Figure 4

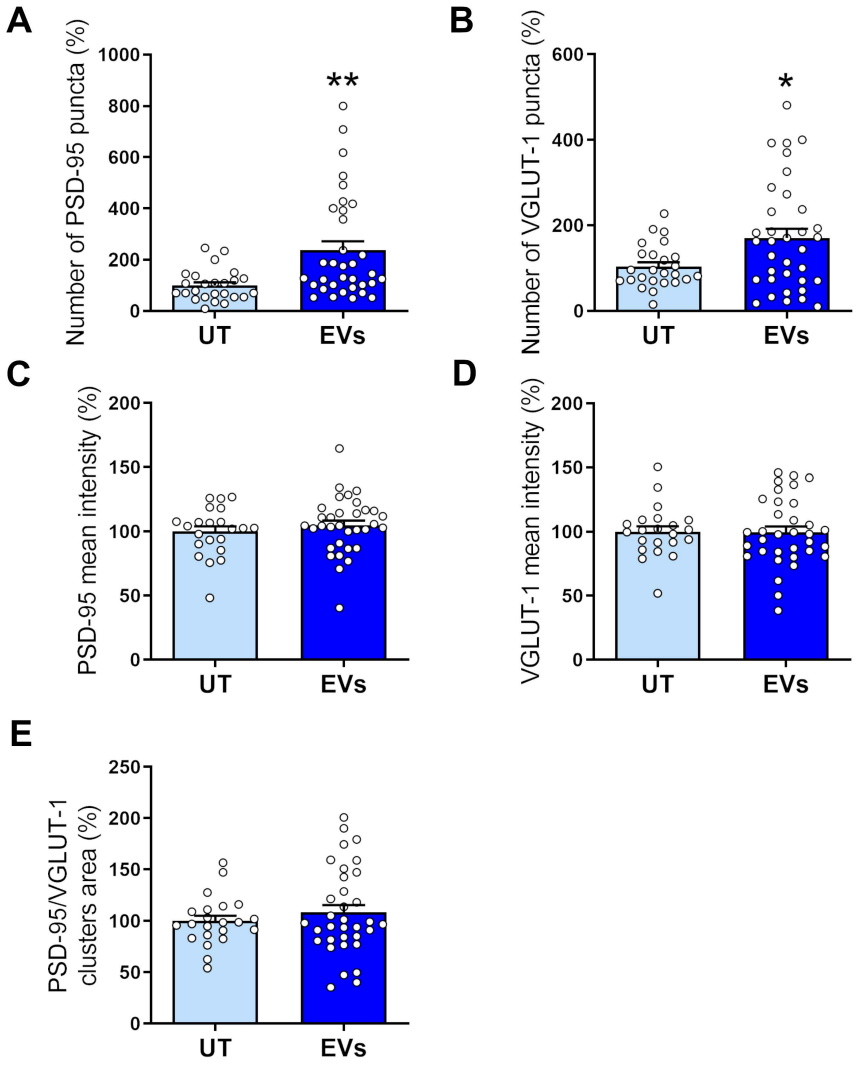

Supplementary Figure 5

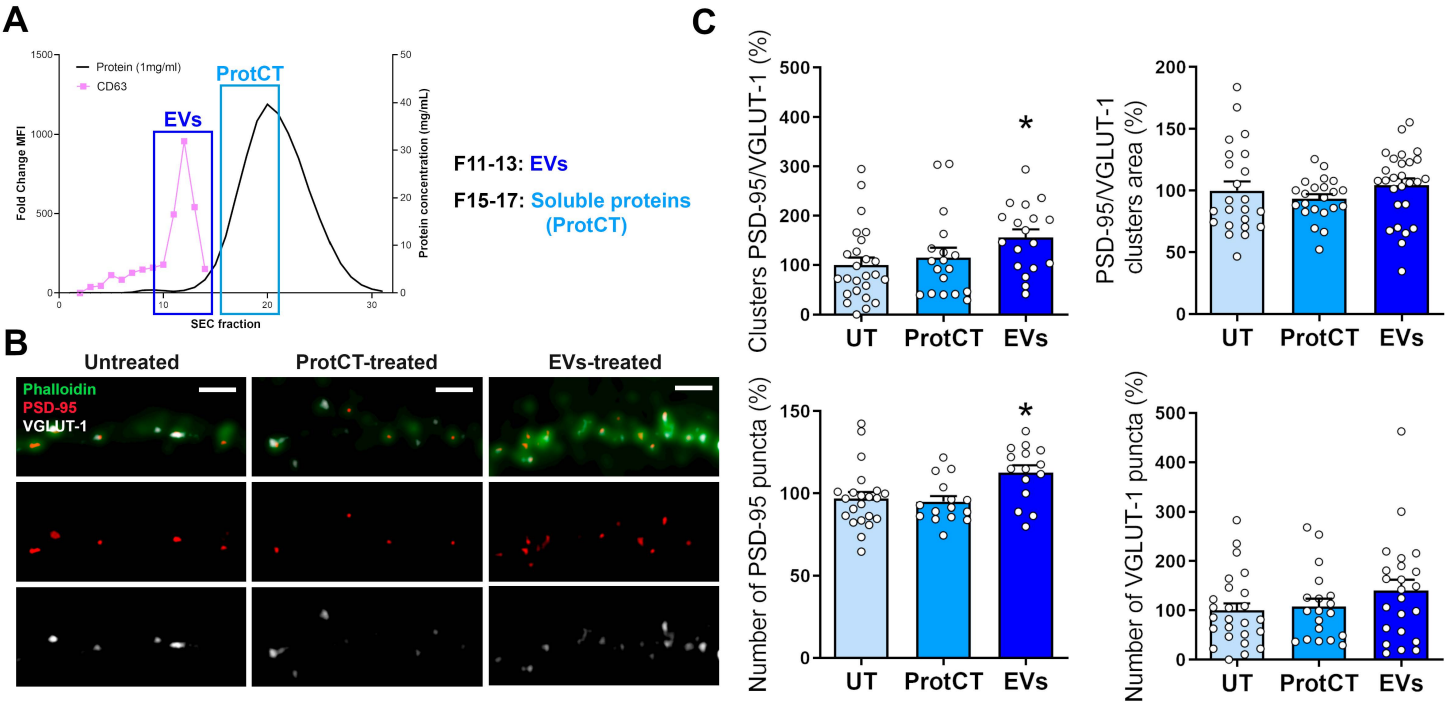

Supplementary Figure 6

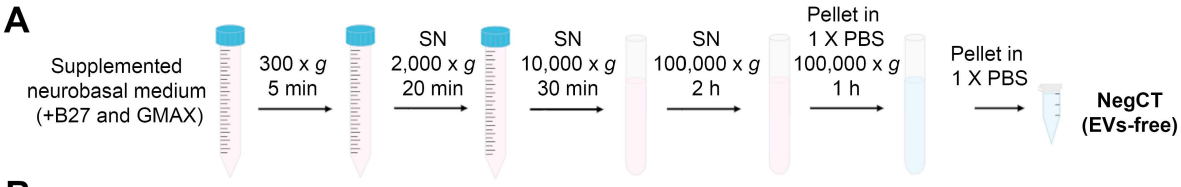

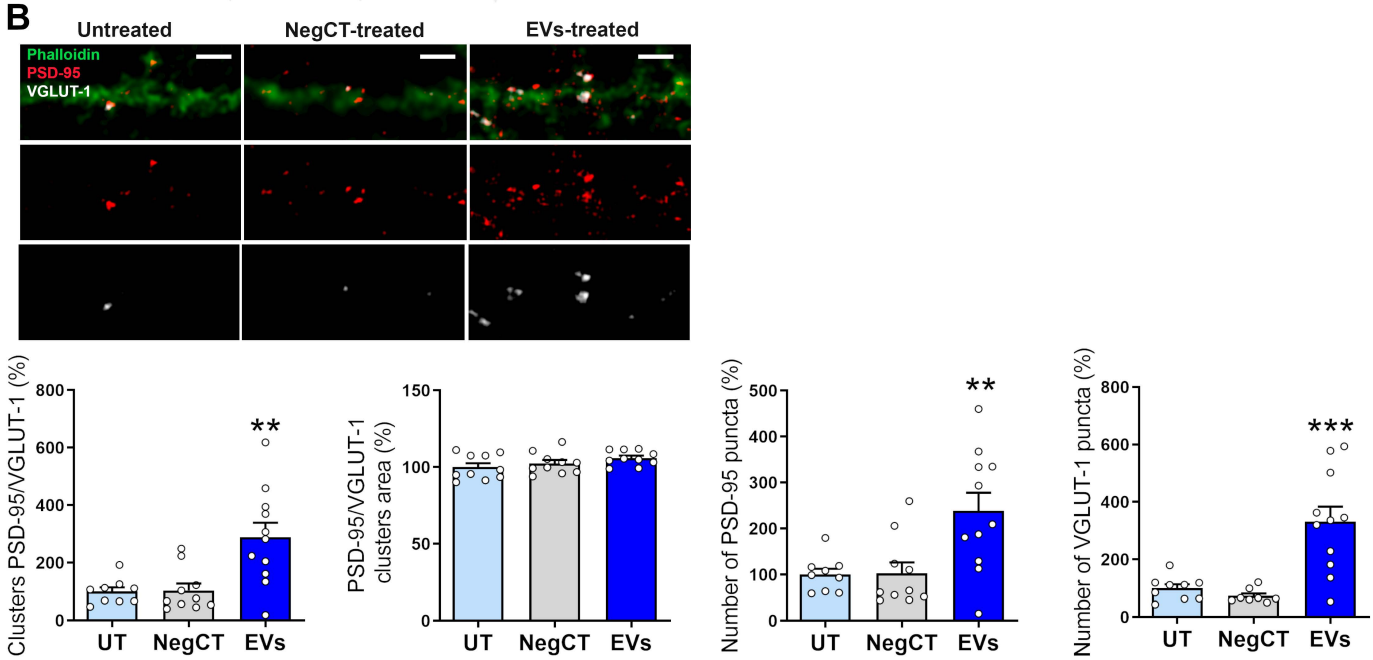

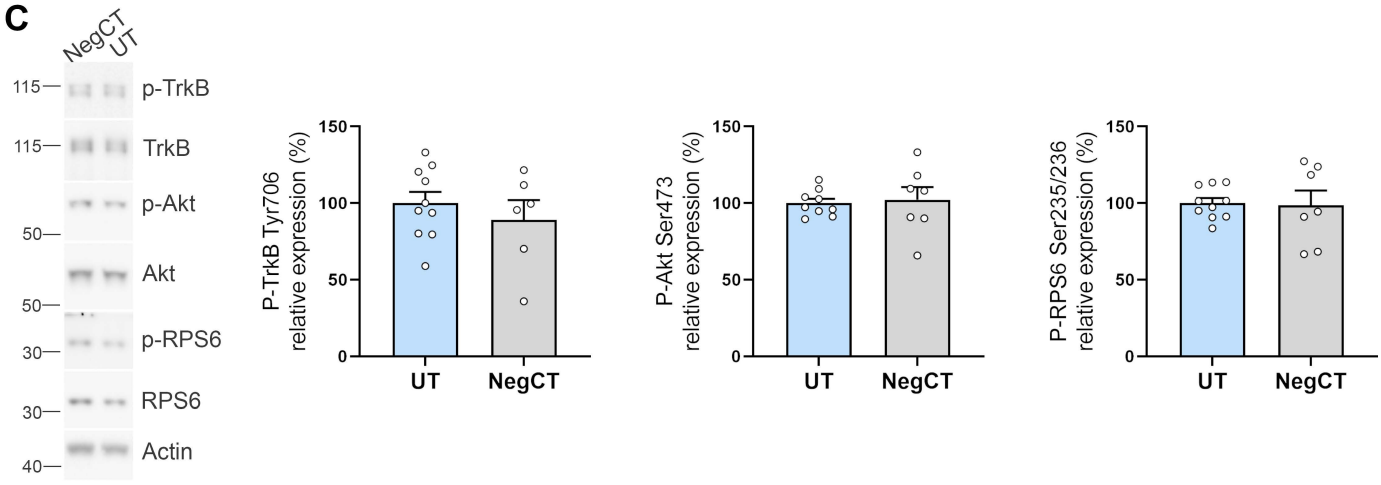

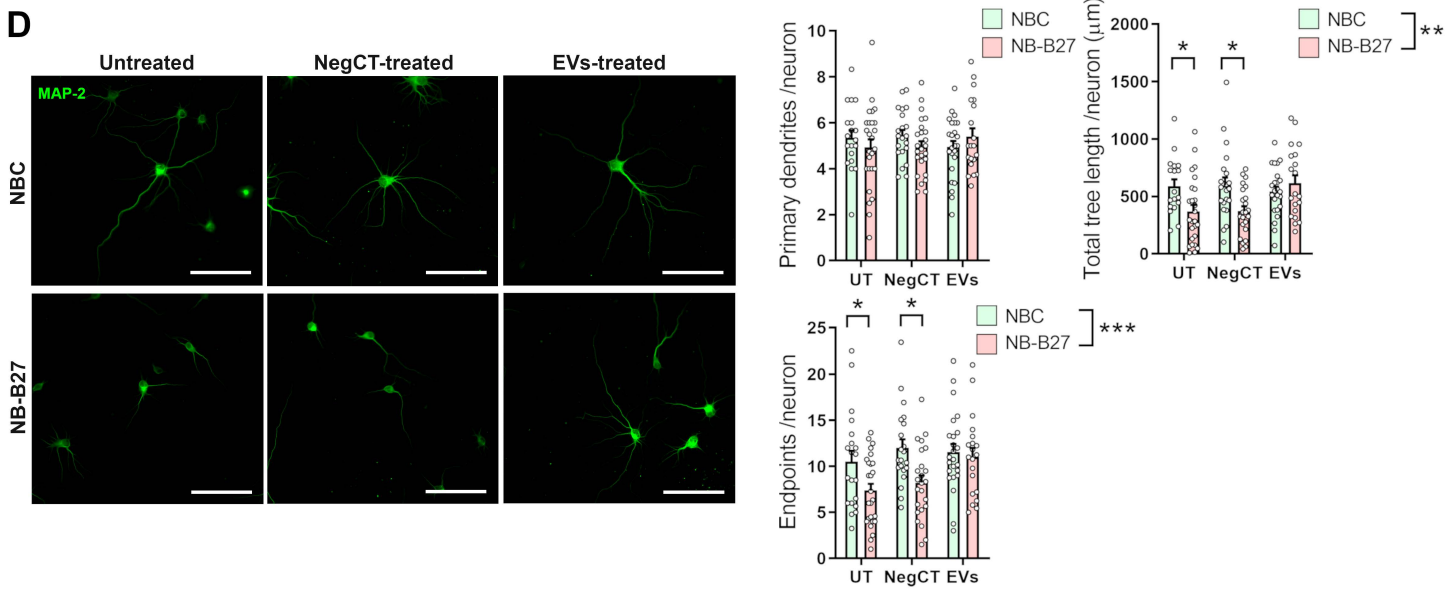

Supplementary Figure 7

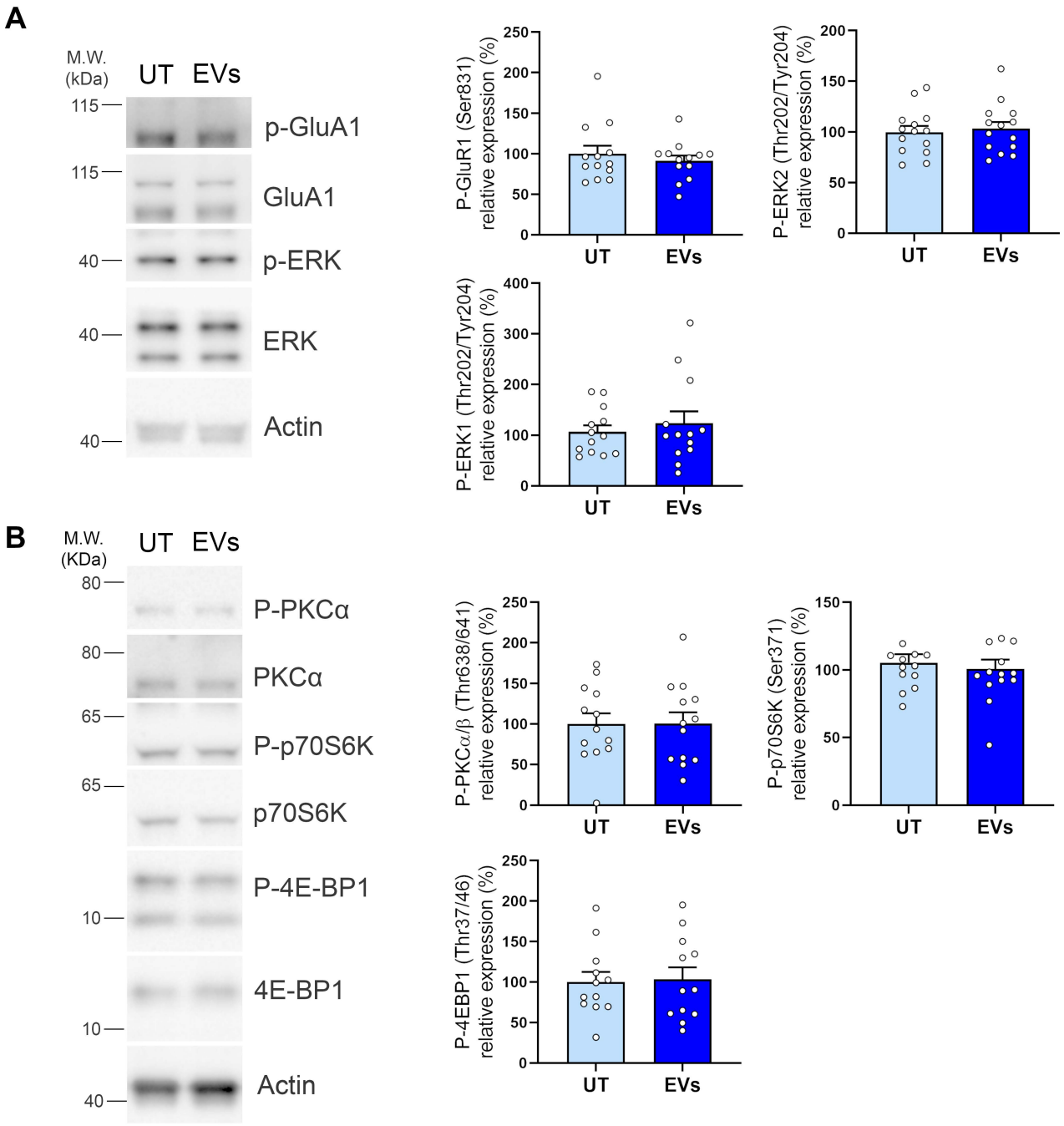

Supplementary Figure 8

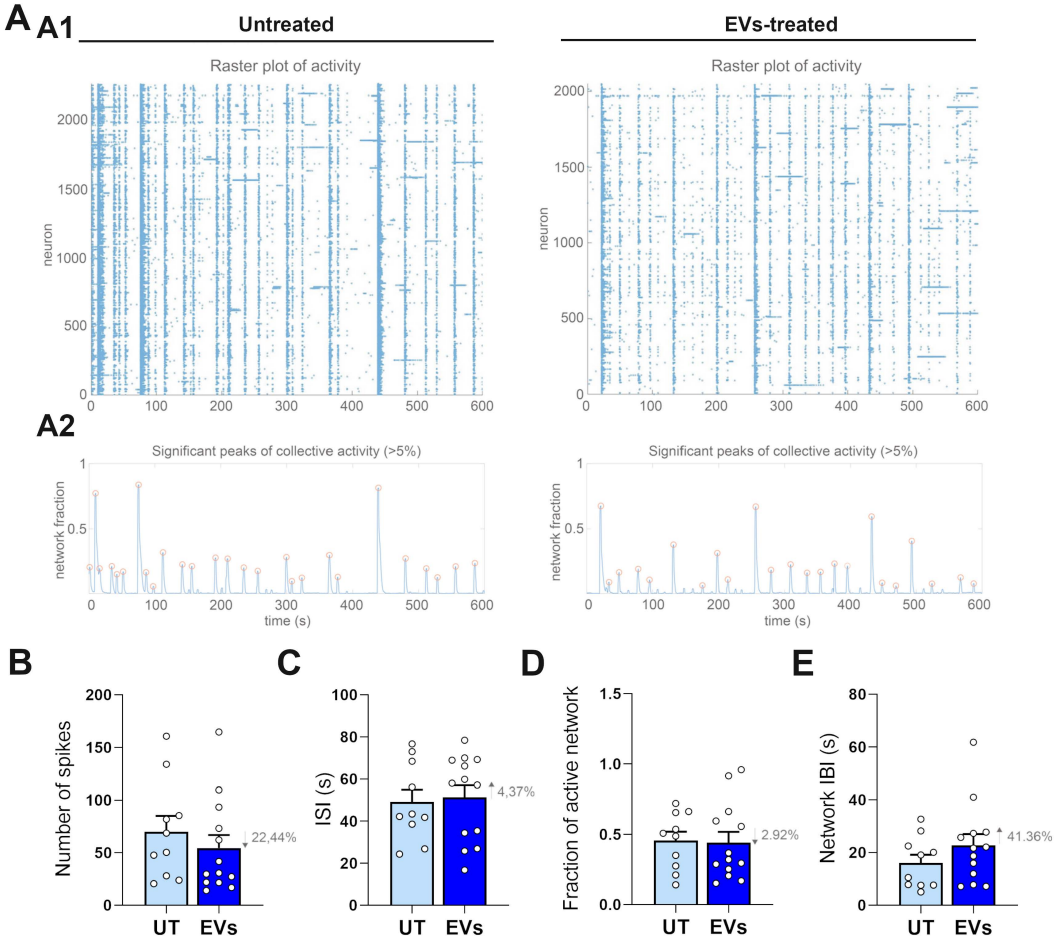

Supplementary Figure 9

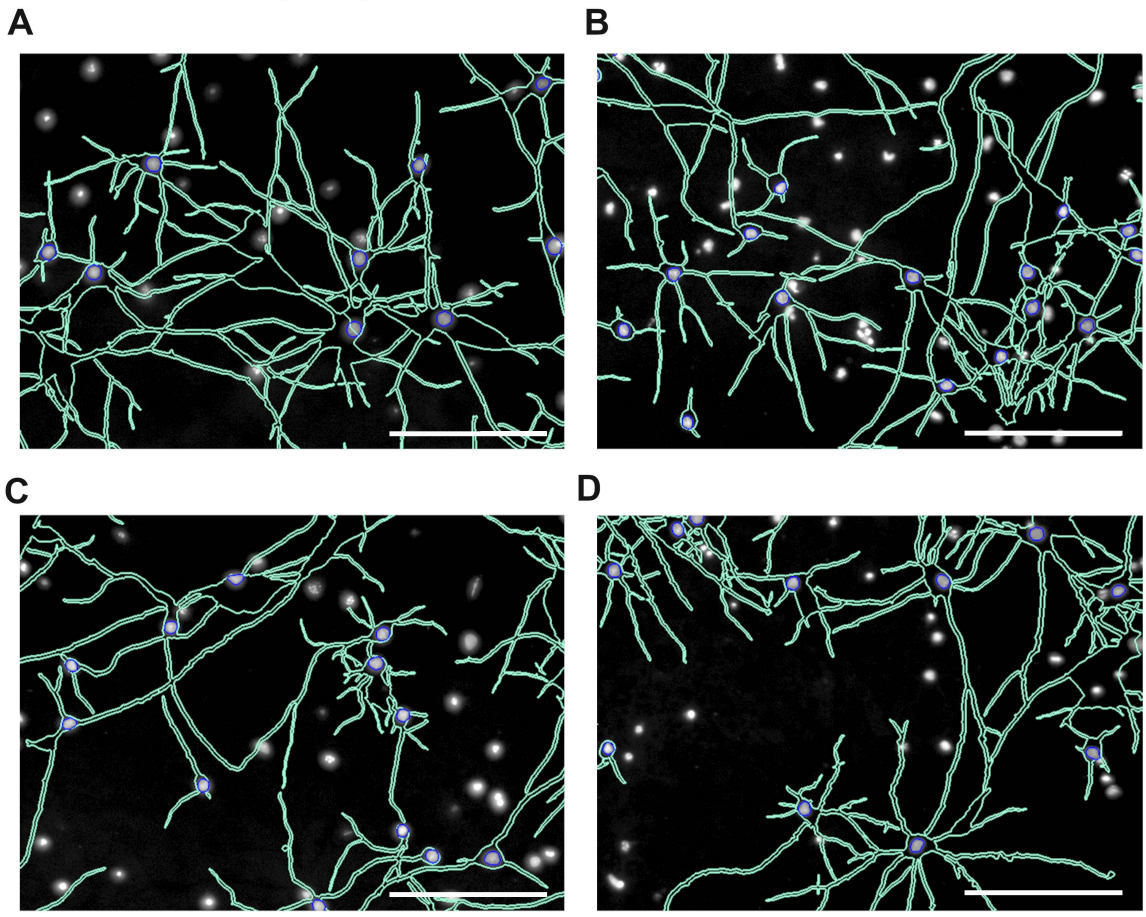

Supplementary Figure 10

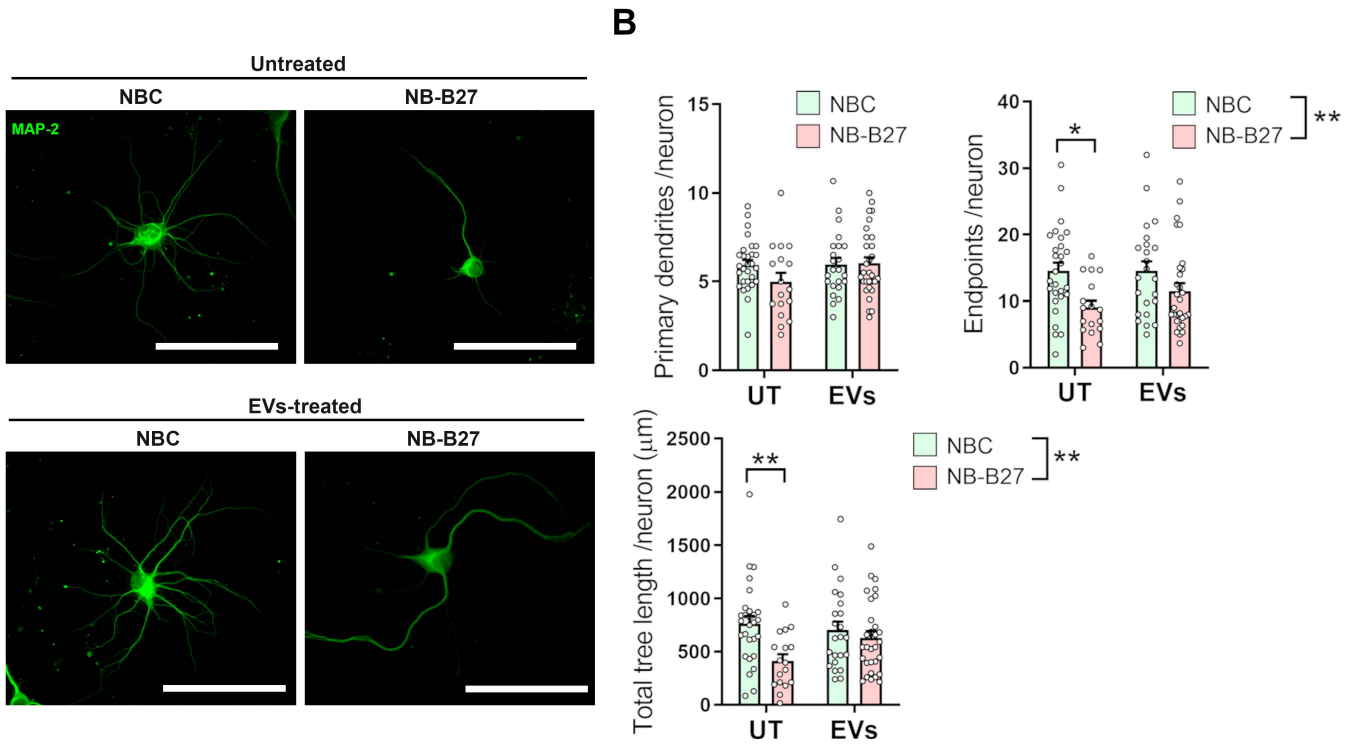

Supplementary Figure 11

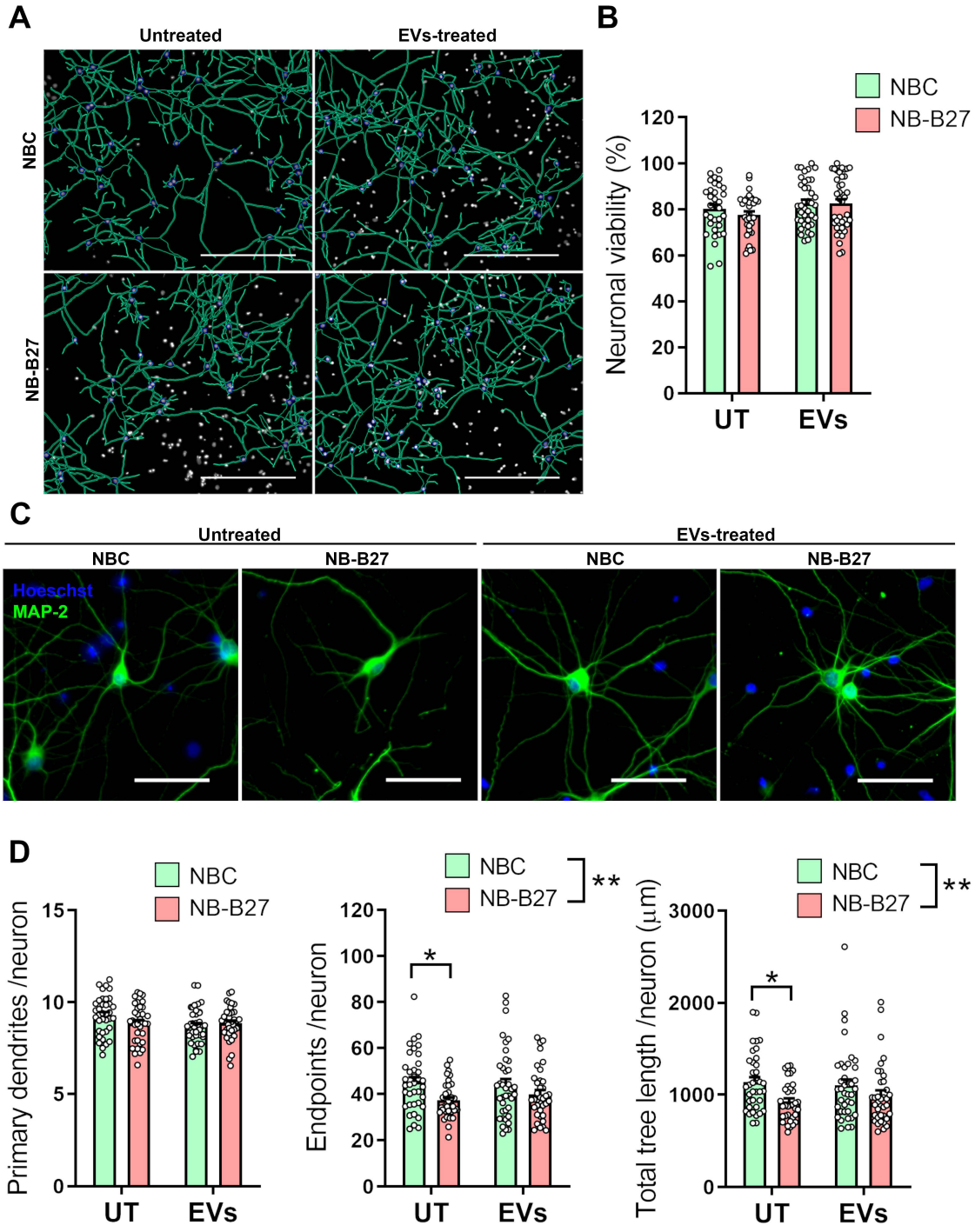

Supplementary Figure 12

Figure 1 (D)

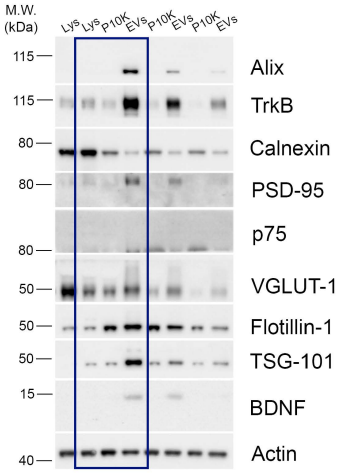

Figure 3 (B1)

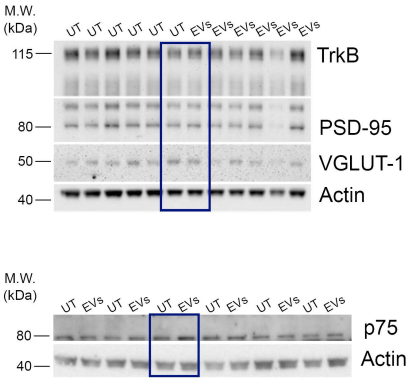

Figure 4 (C)

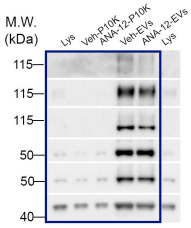

Figure 4 (D1), Figure S6 (C)

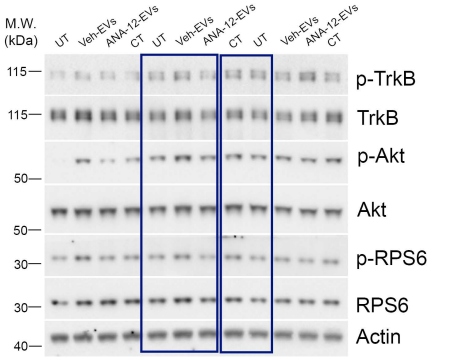

Figure S2 (E)

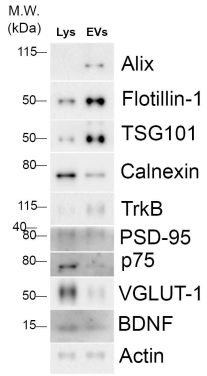

Figure S7